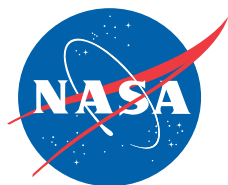


NASA/TM-2009-214646



Updating the Finite Element Model of the Aerostructures Test Wing Using Ground Vibration Test Data

Shun-Fat Lung
TYBRIN Inc.
Edwards, California

Chan-Gi Pak
NASA Dryden Flight Research Center
Edwards, California

April 2009

NASA STI Program ... in Profile

Since its founding, NASA has been dedicated to the advancement of aeronautics and space science. The NASA scientific and technical information (STI) program plays a key part in helping NASA maintain this important role.

The NASA STI program operates under the auspices of the Agency Chief Information Officer. It collects, organizes, provides for archiving, and disseminates NASA's STI. The NASA STI program provides access to the NASA Aeronautics and Space Database and its public interface, the NASA Technical Report Server, thus providing one of the largest collections of aeronautical and space science STI in the world. Results are published in both non-NASA channels and by NASA in the NASA STI Report Series, which includes the following report types:

- **TECHNICAL PUBLICATION.** Reports of completed research or a major significant phase of research that present the results of NASA Programs and include extensive data or theoretical analysis. Includes compilations of significant scientific and technical data and information deemed to be of continuing reference value. NASA counterpart of peer-reviewed formal professional papers but has less stringent limitations on manuscript length and extent of graphic presentations.
- **TECHNICAL MEMORANDUM.** Scientific and technical findings that are preliminary or of specialized interest, e.g., quick release reports, working papers, and bibliographies that contain minimal annotation. Does not contain extensive analysis.
- **CONTRACTOR REPORT.** Scientific and technical findings by NASA-sponsored contractors and grantees.

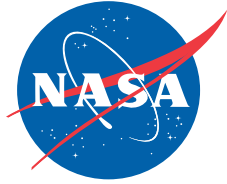
- **CONFERENCE PUBLICATION.** Collected papers from scientific and technical conferences, symposia, seminars, or other meetings sponsored or co-sponsored by NASA.
- **SPECIAL PUBLICATION.** Scientific, technical, or historical information from NASA programs, projects, and missions, often concerned with subjects having substantial public interest.
- **TECHNICAL TRANSLATION.** English-language translations of foreign scientific and technical material pertinent to NASA's mission.

Specialized services also include creating custom thesauri, building customized databases, and organizing and publishing research results.

For more information about the NASA STI program, see the following:

- Access the NASA STI program home page at <http://www.sti.nasa.gov>
- E-mail your question via the Internet to help@sti.nasa.gov
- Fax your question to the NASA STI Help Desk at 443-757-5803
- Phone the NASA STI Help Desk at 443-757-5802
- Write to:
NASA STI Help Desk
NASA Center for AeroSpace Information
7115 Standard Drive
Hanover, MD 21076-1320

NASA/TM-2009-214646



Updating the Finite Element Model of the Aerostructures Test Wing Using Ground Vibration Test Data

*Shun-Fat Lung
TYBRIN Inc.
Edwards, California*

*Chan-Gi Pak
NASA Dryden Flight Research Center
Edwards, California*

*National Aeronautics and
Space Administration*

*Dryden Flight Research Center
Edwards, California 93523-0273*

April 2009

ACKNOWLEDGEMENT

The authors would like to acknowledge the assistance of Claudia Herrera, Matt Moholt and Starr Ginn at NASA Dryden Flight Research Center in the setting and performing of the ground vibration tests.

NOTICE

Use of trade names or names of manufacturers in this document does not constitute an official endorsement of such products or manufacturers, either expressed or implied, by the National Aeronautics and Space Administration.

Available from:

NASA Center for AeroSpace Information
7115 Standard Drive
Hanover, MD 21076-1320
(301) 621-0390

ABSTRACT

Improved and/or accelerated decision making is a crucial step during flutter certification processes. Unfortunately, most finite element structural dynamics models have uncertainties associated with model validity. Tuning the finite element model using measured data to minimize the model uncertainties is a challenging task in the area of structural dynamics. The model tuning process requires not only satisfactory correlations between analytical and experimental results, but also the retention of the mass and stiffness properties of the structures. Minimizing the difference between analytical and experimental results is a type of optimization problem. By utilizing the multidisciplinary design, analysis, and optimization (MDAO) tool in order to optimize the objective function and constraints; the mass properties, the natural frequencies, and the mode shapes can be matched to the target data to retain the mass matrix orthogonality. This approach has been applied to minimize the model uncertainties for the structural dynamics model of the aerostructures test wing (ATW), which was designed and tested at the National Aeronautics and Space Administration Dryden Flight Research Center (Edwards, California). This study has shown that natural frequencies and corresponding mode shapes from the updated finite element model have excellent agreement with corresponding measured data.

NOMENCLATURE

AR	aspect ratio
ATW	aerostructures test wing
CG	center of gravity
DFRC	Dryden Flight Research Center
DOF	degrees of freedom
DPR	driving point residues
d	number of degrees of freedom
<i>E</i>	effective independent matrix
EI	effective independence
F	original objective function
FE	finite element
FIM	Fisher information matrix
G	subscript for target values (or measured quantities)
GA	genetic algorithm
GVT	ground vibration test
g_i	inequality constraints
h_j	equality constraints
I_{XX}	computed x moment of inertia about the center of gravity
I_{XXG}	target x moment of inertia about the center of gravity
I_{xy}	computed xy moment of inertia about the center of gravity
I_{XYG}	target xy moment of inertia about the center of gravity
I_{YY}	computed y moment of inertia about the center of gravity
I_{YYG}	target y moment of inertia about the center of gravity
I_{YZ}	computed yz moment of inertia about the center of gravity
I_{YZG}	target yz moment of inertia about the center of gravity
I_{ZX}	computed zx moment of inertia about the center of gravity

I_{ZXG}	target zx moment of inertia about the center of gravity
I_{ZZ}	computed z moment of inertia about the center of gravity
I_{ZZG}	target z moment of inertia about the center of gravity
J_i	objective functions (optimization problem statement number $i = 1, 2, \dots, 13$)
\mathbf{K}	stiffness matrix
$\overline{\mathbf{K}}$	orthonormalized stiffness matrix
\mathbf{KE}	kinetic energy
KE_{ik}	kinetic energy associated with the i -th DOF in the k -th target mode
L	new objective function
l	number of modes
\mathbf{M}	mass matrix
$\overline{\mathbf{M}}$	orthonormalized mass matrix
MAC	modal assurance criterion
MDAO	multidisciplinary design, analysis and optimization
m	number of sensors (or number of measured degrees of freedom)
n	number of modes to be matched
q	number of inequality constraints
r	number of equality constraints
SEREP	system equivalent reduction expansion process
SMI	structural mode interaction
\mathbf{T}	transformation matrix
W	computed total mass
W_G	target total mass
X	x-coordinate of computed center of gravity
\overline{X}	design variables vector
X_G	x-coordinate of target center of gravity
Y	y-coordinate of computed center of gravity
Y_G	y-coordinate of target center of gravity
Z	z-coordinate of computed center of gravity
Z_G	z-coordinate of target center of gravity
ϵ	small tolerance value for inequality constraints
λ	Lagrange multiplier
Φ	computed eigen-matrix ($m \times n$)
Φ_G	target eigen-matrix ($m \times n$)
$\overline{\Phi}$	Reduced modal matrix ($d \times l$)
ϕ_i	i -th mode shape ($d \times 1$)
Ω_j	j -th computed frequency
ω_k	corresponding natural frequency

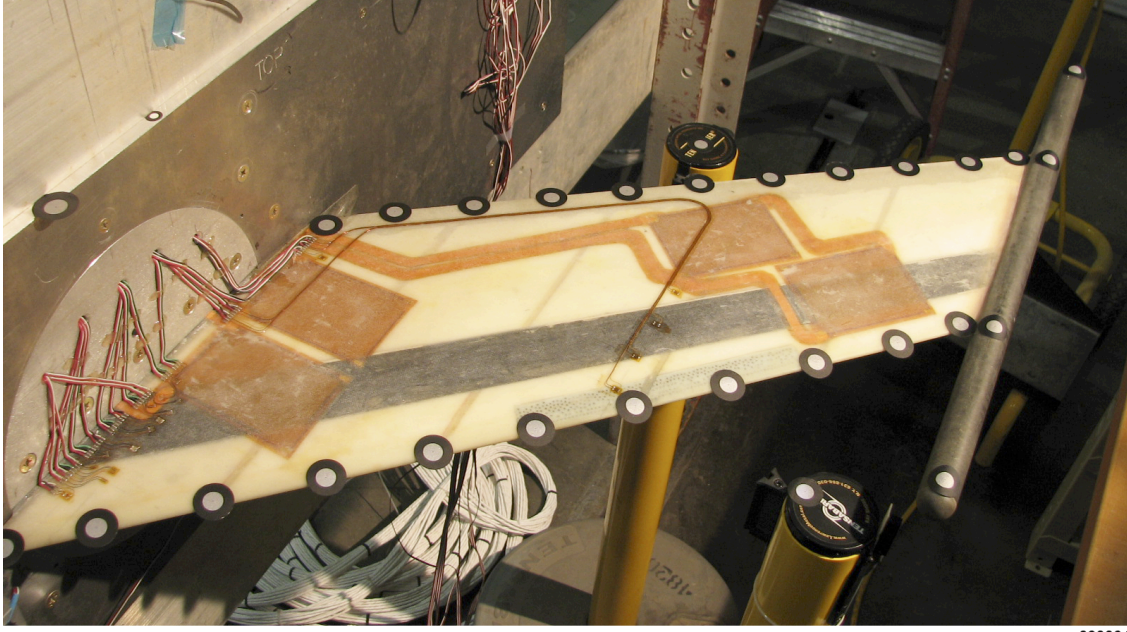
INTRODUCTION

A test article called the aerostructures test wing (ATW) was developed and flown at the National Aeronautics and Space Administration (NASA) Dryden Flight Research Center (DFRC) (Edwards, California) on the McDonnell Douglas NF15B test bed aircraft as shown in figure 1 for the purpose of demonstrating and validating flutter prediction methods during flight (ref. 1). The first aerostructures test wing (ATW1), flown in 2001, was originally developed to directly address requests for better flight flutter test techniques by providing a functional flight test platform. While the first series of tests was extremely successful, the minimum amount of instrumentation (structural accelerometers and strain gages) was chosen to satisfy the scope of the program. These sensors were limited in their capability to answer questions of aeroelastic interactions, sources of nonlinearity, physical mechanisms of aeroelastic coupling, and feedback dynamics between the structure and aerodynamics.



Figure 1. Aerostructures test wing mounted on the NF15B for flight flutter testing.

A second aerostructures test wing (ATW2), as shown in figure 2, was built for the demonstration of state-of-the-art sensor technologies for simultaneous; distributed; collocated measurement of shear stress (skin friction); steady and unsteady pressures; and structural strain and accelerations for mode shapes as well as other modal properties. Like the ATW1, the ATW2 was flown on the NF15B aircraft. In order to have a successful prediction of the onset flutter, the structural dynamics finite element (FE) model has to be robust and accurate. The ground vibration test (GVT) is used as one of the validation methods for robustness of the FE model.



090061

Figure 2. Aerostructures test wing 2.

The primary objective of this study is to obtain the GVT validated structural dynamics FE model for minimizing model uncertainties in the predicted flutter boundaries. Discrepancies are common between the test data and the analytical results. However, the FE model can be fine tuned through the use of the GVT data. Accurate and reliable GVT results are important to this adjusting process. Selection of measurement locations can be critical to the success of an experimental modal survey. So, different sensor and exciter placement algorithms for pre-test evaluations were investigated to ensure the quality of the modal test.

Manual trial-and-error methods provide an inefficient approach to correlate the FE model with test data. A more efficient approach is to use a mode matching technique for the model refinement of both ground and flight-based models. A model tuning technique utilized was NASA Dryden's multidisciplinary design, analysis, and optimization (MDAO) tool (ref. 2), which was used to adjust the structural properties so that the analytical results and the measured data were matched.

SENSOR/ACTUATOR PLACEMENT METHODS

It is important to assure that an adequate number of proper sensor locations are identified for the collection of data during the GVT. There are several existing techniques that can be used for the determination of measurement locations. These algorithms start with a full or selected set of finite element degrees of freedom (DOFs) with the desired number of mode shapes as shown in equation (1):

$$\bar{\Phi} = [\phi_1 \phi_2 \dots \phi_l] \quad (1)$$

where $\bar{\Phi}$ is the reduced modal matrix ($d \times l$). Depending on the algorithm, the unwanted DOFs can be eliminated in one cycle or iteratively until the desired number of sensors is reached.

Effective Independence

The objective of the effective independence (EI) method is to select sensor locations that make the target modes linearly independent, while retaining as much information as possible. This procedure starts from a large set of candidate sensor locations in which the effective independence matrix E can be formed as shown in equation (2) (ref. 3).

$$E = \overline{\Phi} (\overline{\Phi}^T \overline{\Phi})^{-1} \overline{\Phi}^T \quad (2)$$

The DOF with the smallest value is removed and the E matrix is re-calculated for the new candidate set. The iterative process continues until the desired number of sensors is reached.

Genetic Algorithm

Selection of the sensor locations is a kind of optimization problem with discrete design variables. One of the solution methods for this optimization problem is the genetic algorithm (GA) (ref. 4). Using the determinant of the Fisher information matrix (**FIM**) as objective function, and sensor locations as design variables, the optimal sensor locations can be determined. The **FIM** is defined as shown in equation (3) (ref. 5).

$$\mathbf{FIM} \equiv \overline{\Phi}^T \overline{\Phi} \quad (3)$$

The sensor locations, which are based on the desired number of sensors, are randomly picked and the GA method will find the best set of locations that gives the maximum determinant value of the **FIM**. The determinant of the **FIM** indicates the amount of information in the data that is retained at the reduced set of coordinates. Maintaining a high value for this determinant is desired so that the **FIM** retains as much information as possible. The optimization problem statement can be written as:

Maximize the objective function $obj = \det(\mathbf{FIM})$ for any set of sensor positions with no constraint equations.

Kinetic Energy Sorting

The kinetic energy sorting technique involves an examination of each DOF's contribution of kinetic energy to each mode shape. The calculation of the kinetic energy in terms of the mode shapes can be expressed as shown in equation (4):

$$KE_{ik} = \overline{\Phi}_{ik} \sum_j M_{ij} \overline{\Phi}_{jk} \quad (4)$$

where KE_{ik} is the kinetic energy associated with the i -th DOF in the k -th target mode. The total kinetic energy for each DOF is the summation of the normalized kinetic energy of each DOF for each mode. Those DOFs having the greatest contribution or most kinetic energy can be identified and selected as sensor locations.

Guyan Reduction

The purpose of the Guyan reduction (ref. 6) is to remove the number of DOFs in a large FE model, but still maintain the characteristics of the original model at the lower frequencies. Higher frequency modes are neglected because these DOFs can be removed based on the fact that the inertia forces are

negligible compared with the elastic forces. This process involves examining the ratio of stiffness over mass for each DOF. If the ratio is small, then there are significant inertia effects associated with the DOF, and thus it should be retained. If the ratio is large, then the inertia effects are negligible and the corresponding DOF can be removed.

Iterative Guyan Reduction

Unlike the standard Guyan reduction, the iterative Guyan reduction (ref. 7) removes the DOF one at a time so that at each stage the effect of each DOF removed is redistributed to all of the remaining DOFs, resulting in greater accuracy than the non-iterative approach.

Driving Point Residues

Driving point residues (DPR) are equivalent to modal participation factors. They are proportional to the magnitude of the mode shapes. A driving point is a point in the structure where the excitation DOF and the response are equal. If the modal matrix is mass normalized, then the driving point residues for the DOF i of the mode shape k can be computed (ref. 8) as shown in equation (5):

$$DPR_k(i,i) = \frac{\bar{\Phi}(i) \otimes \bar{\Phi}(i)}{\omega_k} \quad (5)$$

where ω_k is the corresponding natural frequency and \otimes is the element-by-element multiplication operator. The normalized DPR can then be used to calculate the average, minimum, maximum, and weighted modal displacement of all the target modes. The optimal sensor/exciter locations are then selected based on the values of the weighted driving point residue and the number of sensors/actuators available for the test. In this study, the weighted minimum was used for the selection of the sensor locations in order to opt out of those DOFs at the nodal point of a mode. The weighted minimum DPR was obtained as shown in equation (6).

$$DPR_{weighted}(i) = \min_{j=1}^n \overline{DPR}_j(i,i) \cdot \frac{1}{n} \sum_{j=1}^n \overline{DPR}_j(i,i) \quad (6)$$

The weighted maximum was used for the selection of the excitation locations so that those easily excited DOFs could be identified. The weighted maximum DPR can be expressed as shown in equation (7):

$$DPR_{weighted}(i) = \max_{j=1}^n \overline{DPR}_j(i,i) \cdot \frac{1}{n} \sum_{j=1}^n \overline{DPR}_j(i,i) \quad (7)$$

where \overline{DPR} is the normalized DPR.

STRUCTURAL DYNAMIC MODEL TUNING PROCEDURE

Discrepancies in frequencies and mode shapes are minimized using a series of optimization procedures (refs. 9-11). There are two optimization algorithms adopted in NASA Dryden's MDAO tool: the traditional gradient-based algorithm (ref. 12) and the genetic algorithm. Gradient-based algorithms work well for continuous design variable problems, whereas GAs can handle continuous and discrete design variable problems easily. When there are multiple local minima, GAs are able to find the global

optimum results, whereas gradient-based methods may converge to a locally minimum value. In this research work, the GA was used for the solution of the optimization problem.

The GA is directly applicable only to unconstrained optimization; it is necessary to use some additional methods in order to solve the constrained optimization problem. The most popular approach is to add penalty functions in proportion to the magnitude of constraint violation to the objective function (ref. 13). The general form of the penalty function is shown in equation (8):

$$L(\bar{X}) = F(\bar{X}) + \sum_{i=1}^q \lambda_i g_i(\bar{X}) + \sum_{j=1}^r \lambda_{j+q} h_j(\bar{X}) \quad (8)$$

where $L(\bar{X})$ indicates the new objective function to be optimized, $F(\bar{X})$ is the original objective function, $g_i(\bar{X})$ is the inequality constraint, $h_j(\bar{X})$ is the equality constraint, λ_i are the Lagrange multipliers, \bar{X} is the design variables vector, and q and r are the number of inequality and equality constraints, respectively.

The analytical mass properties, the mass matrix orthogonality, and the natural frequencies and mode shapes are matched to the target values based on the following three tuning steps.

Step 1: Tuning Mass Properties

The difference in the analytical and target values of the total mass, the center of gravity (CG) location, and the mass moment of inertias at the CG location are minimized to have the improved rigid body dynamics as shown in equations (9) through (18).

$$J_1 = (W - W_G)^2 / W_G^2 \quad (9)$$

$$J_2 = (X - X_G)^2 / X_G^2 \quad (10)$$

$$J_3 = (Y - Y_G)^2 / Y_G^2 \quad (11)$$

$$J_4 = (Z - Z_G)^2 / Z_G^2 \quad (12)$$

$$J_5 = (I_{XX} - I_{XXG})^2 / I_{XXG}^2 \quad (13)$$

$$J_6 = (I_{YY} - I_{YYG})^2 / I_{YYG}^2 \quad (14)$$

$$J_7 = (I_{ZZ} - I_{ZZG})^2 / I_{ZZG}^2 \quad (15)$$

$$J_8 = (I_{XY} - I_{XYG})^2 / I_{XYG}^2 \quad (16)$$

$$J_9 = (I_{YZ} - I_{YZG})^2 / I_{YZG}^2 \quad (17)$$

$$J_{10} = (I_{ZX} - I_{ZXG})^2 / I_{ZXG}^2 \quad (18)$$

Step 2: Tuning Mass Matrix

The off-diagonal terms of the orthonormalized mass matrix are reduced to improve the mass orthogonality as shown in equation (19):

$$J_{11} = \sum_{i=1, j=1, i \neq j}^n (\overline{\mathbf{M}}_{ij})^2 \quad (19)$$

where n is the number of modes to be matched and $\overline{\mathbf{M}}$ is defined as shown in equation (20).

$$\overline{\mathbf{M}} = \Phi_G^T \mathbf{T}^T \mathbf{M} \mathbf{T} \Phi_G \quad (20)$$

In equation 20 above, the mass matrix \mathbf{M} is calculated from the FE model, while the target eigen-matrix Φ_G is measured from the GVT. The eigen-matrix Φ_G remains constant during the optimization procedure. A transformation matrix \mathbf{T} in the above equation is based on Guyan reduction, improved reduction system (ref. 14) or the system equivalent reduction expansion process (SEREP) (ref. 15). This reduction is required due to the limited number of available sensor locations and difficulties in measuring the rotational DOFs.

Step 3: Tuning Frequencies and Mode Shapes

Two different types of approach can be used for tuning the frequencies and mode shapes. In the first option, shown in equations (21) and (22), the objective function considered combines the normalized errors between GVT and computed frequencies with the total error associated with the off-diagonal terms of the orthonormalized stiffness matrix.

$$J_{12} = \sum_{i=1}^n \left(\frac{\Omega_i - \Omega_{iG}}{\Omega_i} \right)^2 \quad (21)$$

$$J_{13} = \sum_{i=1, j=1, i \neq j}^n (\overline{\mathbf{K}}_{ij})^2 \quad (22)$$

The matrix $\overline{\mathbf{K}}$ is obtained from the matrix products as shown in equation (23):

$$\overline{\mathbf{K}} = \Phi_G^T \mathbf{T}^T \mathbf{K} \mathbf{T} \Phi_G \quad (23)$$

where the stiffness matrix, \mathbf{K} , is calculated from the FE model.

In the second option, shown in equations (24) and (25), the error norm combines the normalized error between the GVT and computed frequencies with the total error between the GVT and computed mode shapes at given sensor points.

$$J_{12} = \sum_{i=1}^n \left(\frac{\Omega_i - \Omega_{iG}}{\Omega_i} \right)^2 \quad (24)$$

$$J_{13} = \sum_{i=1}^m \sum_{j=1}^n (\Phi_{ij} - \Phi_{ijG})^2 \quad (25)$$

In this study, the second option for tuning frequencies and mode shapes was employed since the definition of the objective function is much simpler than in the first option for this application. Any errors in both the modal frequencies and the mode shapes are minimized by including an index for each of these in the objective function. For this option, a small number of sensor locations can be used at which errors between the GVT and computed mode shapes are obtained. Any one of J_1 thru J_{13} can be used as the objective function with the others treated as constraints. This gives the flexibility to achieve the particular

optimization goal while maintaining the other properties as close to the desired target value as possible. The optimization problem statement can be written as:

$$\begin{aligned} &\text{Minimize } J_i \\ &\text{Such that } J_k \leq \epsilon_k, \text{ for } k = 1 \text{ thru } 13 \text{ and } k \neq i \end{aligned}$$

where ϵ_k is a small value which can be adjusted according to the tolerance of each constraint condition.

TEST ARTICLE

The ATW2 was used to demonstrate NASA Dryden's MDAO tool through the process of ground vibration testing and the model tuning technique. This test article was a small-scale airplane wing comprised of an airfoil and wing tip boom as shown in figure 3, based on the ATW1 design. This wing was formulated based on a NACA-65A004 airfoil shape with a 3.28 aspect ratio. The wing had a half span of 18 in. with root chord length of 13.2 in. and tip chord length of 8.7 in. The total area of this wing was 197 in². The wing tip boom was a 1-in. diameter hollow tube of 21.5 in. length. The total weight of the wing was 2.66 lb.

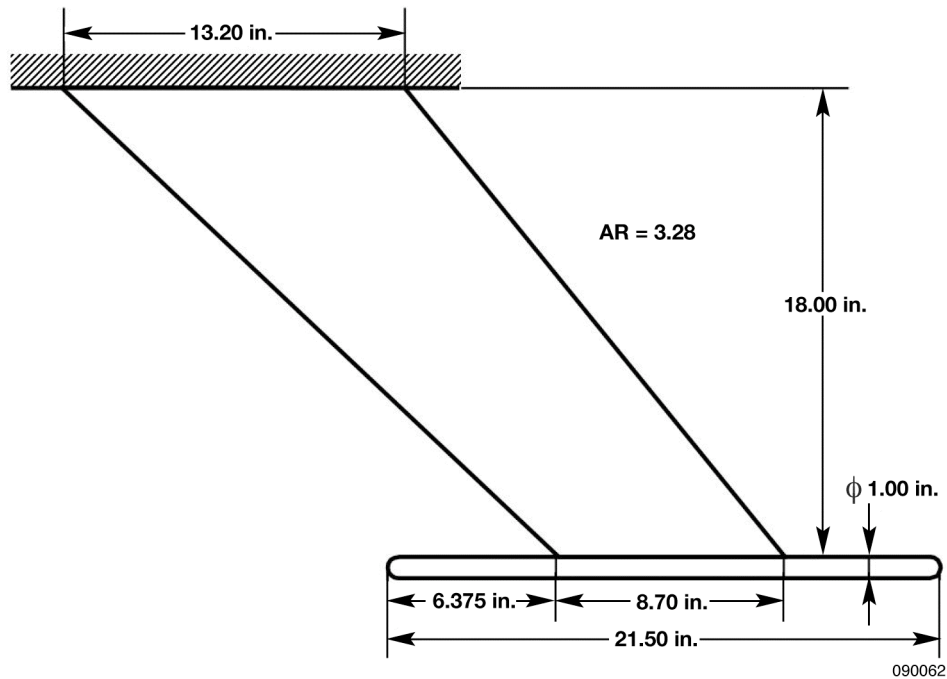


Figure 3. Dimension of the ATW2.

Since the ATW was attached to the F15B flight test fixture, the construction of the wing was limited to lightweight materials with no metal, due to safety concerns. The wing and spar were constructed from fiberglass cloth, the boom was constructed from carbon fiber composite, the wing core was constructed from rigid foam, and the components were attached by epoxy. The wing skin was made of three plies of fiberglass cloth, each about 0.01 in. thick. The internal spar located at the 30% chord line was composed of 10 plies, 0.05 in. thick of carbon at the root but decreases to 1 ply, 0.005 in. thick at the tip.

TEST SETUP

Ground vibration tests were performed to determine the dynamic modal characteristics of the ATW2. In the test set up, the ATW2 was clamped on to a circular plate, which was bolted to a mounting panel, and then installed into a small strong back called the ground test fixture in the NASA Dryden Flight Loads Laboratory. The PONTOS photogrammetry optical measuring system (Gesellschaft für Optische Messtechnik, Braunschweig, Germany), as shown in figure 4, was used to measure output displacement/acceleration at the sensor points. For the excitation method, an impact hammer with an impedance head was used to excite the ATW2's natural frequencies and mode shapes as well as to measure input forces.



Figure 4. The PONTOS photogrammetry optical measuring system.

PONTOS is a non-contact optical 3D measuring system. It analyzes, computes, and documents object deformations, rigid body movements, and the dynamic behavior of a measuring point (ref. 16). The PONTOS system provides an alternative for complex sensor technology like laser sensor, draw-wire sensors or accelerometers, which are commonly used in GVTs for measuring responses of the structure. The features of the PONTOS system include:

- Unlimited number of sensors. The sensor markers are weightless, and a large number of sensors can be used at the same time without altering the total weight or the mode shapes of the structure.
- Non-contact acquisition of the precise 3D position of any number of measuring points.
- Mobility and flexibility due to an easy and compact measuring system.
- Easy and quick adaptation to different measuring volumes and measuring tasks.

The limitations of the PONTOS system include:

- Measuring structural vibration up to 250 Hz.
- Measuring frame rate up to 500 Hz at 1280x1024 pixels.
- Measuring volume up to 1700x1360x1360 mm³.
- Applying the sensors on a plane or slightly curved surface.

SENSOR PLACEMENT DISCUSSION

Only a small number of sensors were placed on the wing for the GVT compared to the full FE model DOFs. The selection of sensor locations were based on the sensor placement algorithms previously discussed in Section II. In order to compare different sensor placement algorithms, the determinant of **FIM** was calculated for different sets of sensor locations. Results are summarized in table 1 and the corresponding sensor locations are shown in figure 5.

Table 1. Comparison of the determinant of FIM for different sensor placement algorithm.

Sensor placement algorithms	det(FIM) (30 sensors, 3 modes)
Effective independence	753.1
Genetic algorithm*	753.1
Kinetic energy	303.6
Iterative Guyan reduction	59.5
Non-iterative Guyan reduction	8.6
Model configuration (25 sensors)	50.0
Driving point residue	97.0

* Based on 150 populations and 500 generations

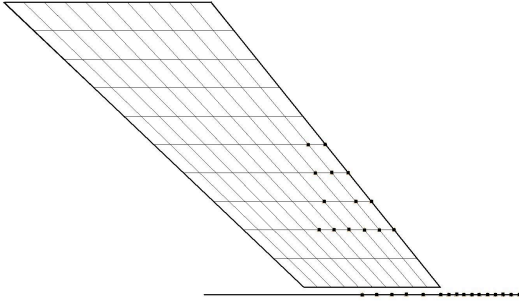


Figure 5a. DPR method.

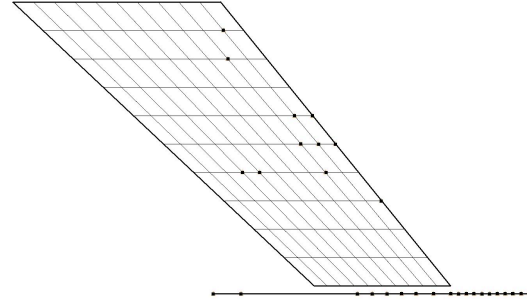


Figure 5b. KE method.

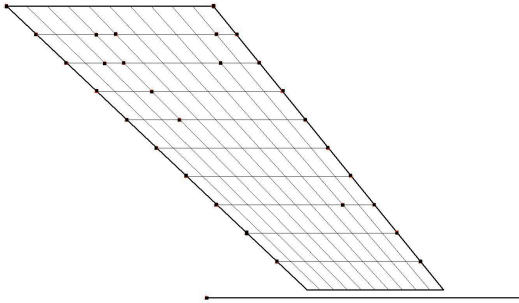


Figure 5c. Guyan reduction method.

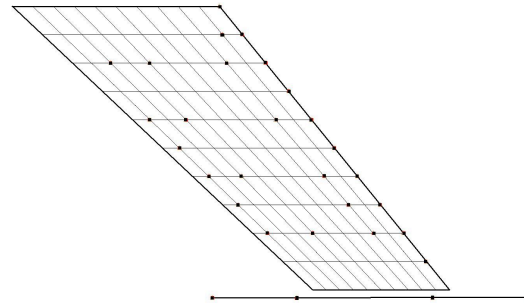


Figure 5d. Iterative Guyan reduction method.

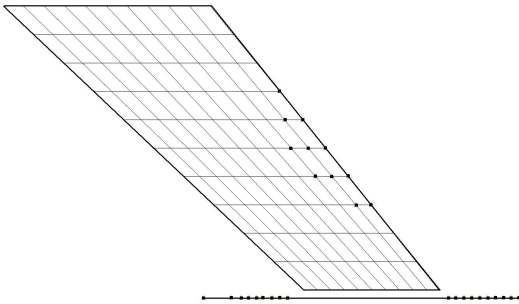


Figure 5e. Effective independence method.

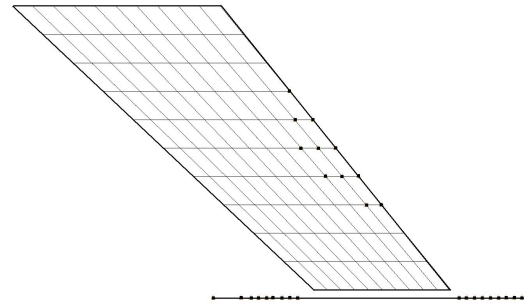


Figure 5f. Genetic algorithm.

090064

Figure 5. Sensor locations from different sensor placement algorithms.

In table 1, the EI and GA methods have the same determinant of **FIM** value. This is due to the fact that the EI method is also an optimization process. In this application, both the EI and GA methods found the globally optimal value. The sensor locations with higher determinant of **FIM** value were used for the GVT response measurement locations.

For the excitation point selection, the weighted maximum driving point residue method was used to determine the excitation locations. The predicted sensor locations and excitation point based on the FE model of the ATW2 is shown in figure 6 and the corresponding coordinates are given in table 2.

At the time of this ATW2 research work, only the GVT results with the sensor placements based on the model configuration were available. Therefore, these data were used for the FE model tuning process.

The sensor locations and excitation point of this GVT are shown in figure 7, and its coordinates are listed in table 3. Figure 8 shows the typical time history and frequency response curves of the ATW2 ground vibration tests.

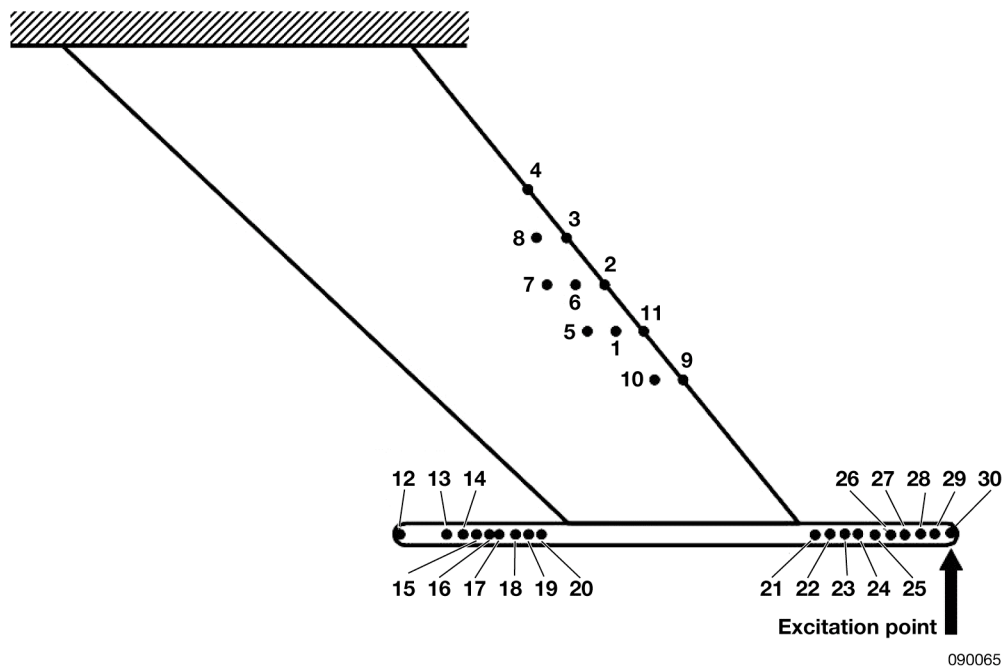


Figure 6. Predicted sensor/excitation locations.

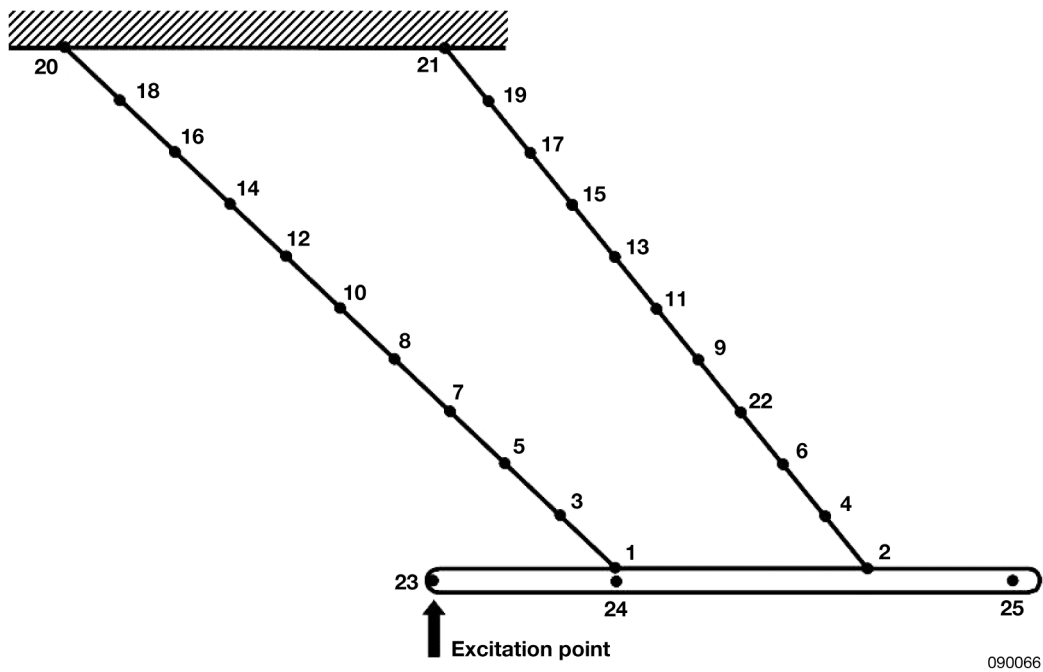


Figure 7. GVT sensor/excitation locations.

Table 2. Sensor locations for Figure 6.

Sensor point	Coordinates (inch)		
	X	Y	Z
1	20.9244	-10.80	-0.05
2	21.9750	-10.80	0
3	19.0499	-7.20	0
4	17.5875	-5.40	-0.001
5	19.8735	-10.80	0.1016
6	19.4167	-9.00	0.0537
7	18.3209	-9.00	0.1059
8	17.9092	-7.20	0.0559
9	23.4375	-12.60	0
10	22.4317	-12.60	0.0493
11	21.9750	-10.80	0
12	12.7500	-18.50	0
13	14.5000	-18.50	0
14	15.1250	-18.50	0
15	15.6250	-18.50	0
16	16.1250	-18.50	0
17	16.5000	-18.50	0
18	17.1250	-18.50	0
19	17.6250	-18.50	0
20	18.1250	-18.50	0
21	28.3250	-18.50	0
22	28.8250	-18.50	0
23	29.3250	-18.50	0
24	29.8250	-18.50	0
25	30.3250	-18.50	0
26	30.8250	-18.50	0
27	31.3250	-18.50	0
28	31.8250	-18.50	0
29	32.3250	-18.50	0
30	32.8250	-18.50	0

Table 3. Sensor locations for Figure 7.

Sensor point	Coordinates (inch)		
	X	Y	Z
1	19.125	-18.00	0
2	27.825	-18.00	0
3	17.212	-16.20	0
4	26.362	-16.20	0
5	15.300	-14.40	0
6	24.900	-14.40	0
7	13.387	-12.56	0
8	11.475	-10.80	0
9	21.975	-10.80	0
10	9.5625	-9.00	0
11	20.5125	-9.0	0
12	7.65	-7.2	0
13	19.0499	-7.2	0
14	5.7375	-5.4	0
15	17.5875	-5.4	0
16	3.825	-3.6	0
17	16.125	-3.6	0
18	1.9125	-1.8	0
19	14.6625	-1.8	0
20	0	0	0
21	13.2	0	0
22	23.4375	-12.6	0
23	12.75	-18.5	0
24	19.125	-18.5	0
25	32.825	-18.5	0

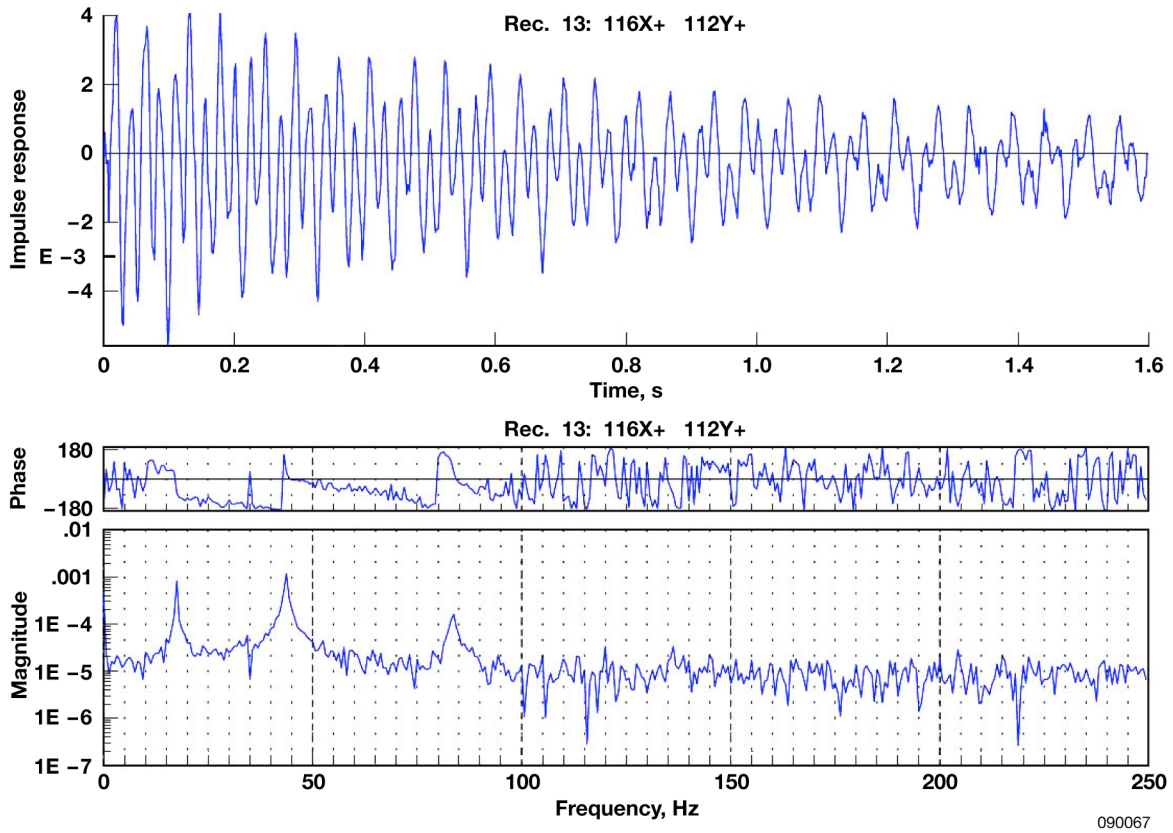


Figure 8. Typical time history and frequency response GVT results for the ATW2.

MODEL TUNING

The frequencies and mode shapes of first bending, first torsion and second bending modes; and total mass from the GVT are listed in table 4. The measurements of table 4 were based on the time history responses data collected by the PONTOS system at each of the sensor points. The eigensystem realization algorithm routine, which was developed by Juang and Pappa (ref. 17) at NASA Langley Research Center (Hampton, Virginia), was then used to identify the frequencies and mode shapes of the system.

Table 4. Measured frequencies and mode shapes (Z direction).

Sensor point	Mode 1 (17.24 Hz)	Mode 2 (44.10 Hz)	Mode 3 (84.00 Hz)
1	0.481	-0.398	-0.325
2	0.755	0.409	-0.187
3	0.386	-0.390	-0.149
4	0.670	0.353	0.142
5	0.311	-0.408	0.088
6	0.589	0.254	0.455
7	0.214	-0.320	0.113
8	0.139	-0.252	0.157
9	0.368	0.082	0.912
10	0.085	-0.177	0.131
11	0.281	0.036	1.000
12	0.047	-0.116	0.140
13	0.196	0.021	0.917
14	0.018	-0.067	0.053
15	0.157	0.018	0.870
16	0.006	0.022	-0.012
17	0.081	0.026	0.587
18	0.008	0.007	0.006
19	0.035	0.025	0.345
20	0.010	0.008	0.017
21	0.014	0.022	0.125
22	0.451	-0.111	0.765
23	0.312	-1.000	-0.582
24	0.518	-0.432	-0.523
25	1.000	0.962	-0.196

Corresponding numerical FE model frequencies and mode shapes computed using MSC/NASTRAN (MSC. Software Corporation, Santa Ana, California) (ref. 18) are shown in figure 9. The FE model in the MSC/NASTRAN format is provided in the appendix. The frequency differences between the GVT and the numerical results before model tuning (shown in table 5) were 53% in the second mode and 12% in the third mode, both of which greatly exceed the 3% limitation for the primary modes allowed by military specifications (refs. 19, 20). Therefore, the FE model needs to be updated for a more reliable flutter analysis.

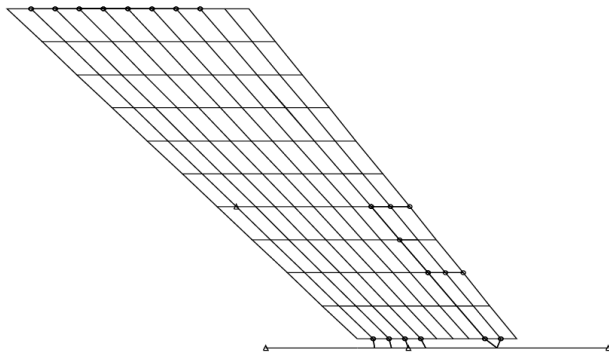


Figure 9a. MSC/NASTRAN FE model.

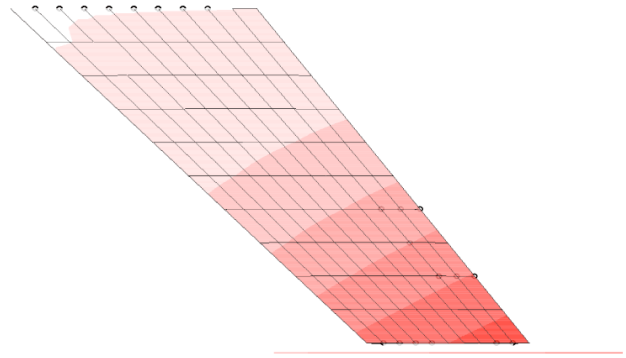


Figure 9b. Mode 1 (1st bending): 17.7048 Hz.

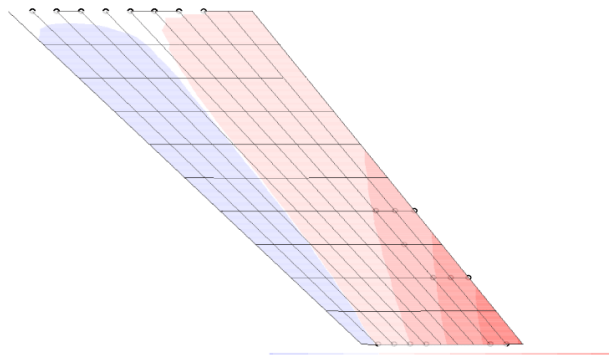


Figure 9c. Mode 2 (1st torsion): 20.9207 Hz.

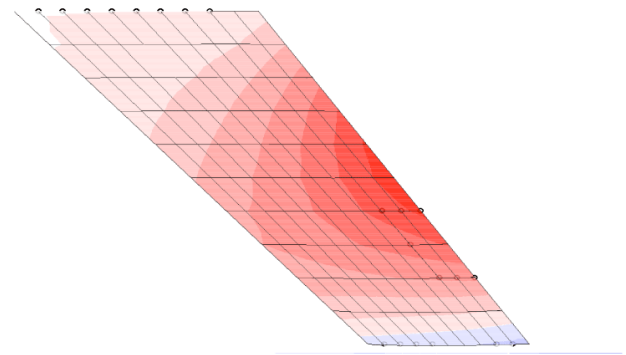


Figure 9d. Mode 3 (2nd bending): 88.3203 Hz.

090068

Figure 9. Finite element model and mode shapes before tuning.

Table 5. Frequencies and total weight of the ATW2 before and after model tuning.

	GVT (Hz)	Before		After	
		MSC/NASTRAN (Guyan/Full; Hz)	Error (%)	MSC/NASTRAN (SEREP/Full; Hz)	Error (%)
Mode 1	17.24	17.71/17.70	2.72/2.68	17.79/17.79	3.19/3.19
Mode 2	44.10	20.93/20.92	-52.5/-52.6	44.71/44.71	1.38/1.38
Mode 3	84.00	93.91/88.32	11.80/5.14	84.33/84.33	0.39/0.39
Total weight (lb)	2.66	2.77	4.13	2.72	2.25

Since Guyan reduction is a static condensation, it is only accurate for lower modes. For higher modes, the errors become too large as shown in table 5. Unlike the Guyan reduction, the SEREP process preserves the dynamic character of the original full system model for selected modes of interest. Therefore the dynamic characteristics of the reduced model were virtually the same as the full model shown in table 5. Therefore, the SEREP model reduction process was used in this ATW2 model update application.

Using frequency difference as an objective function; and mass properties, mass orthogonality, and mode shapes as constraint equations; the frequencies before and after model tuning are presented in table

5. Dramatic improvement was noted, in that after model tuning, the frequencies difference was reduced to 1.38% in the second mode and 0.39% in the third mode.

Table 6 shows the center of gravity, moment of inertia, orthonormalized mass matrix, and modal assurance criterion (MAC) values of the ATW2 before and after model tuning. The off-diagonal terms of the orthonormalized mass matrix, maximum of 37% before model tuning, were minimized in the second tuning step. The maximum off-diagonal term of 7.4% after model tuning is observed in table 6, and this off-diagonal term of the orthonormalized mass matrix satisfies the 10% limitation allowed by military specifications. Model correlation with the test data prior to model tuning was poor and unacceptable to proceed with flight. The MAC values of 0.52 and 0.73 for modes 2 and 3 before model tuning become 0.97 and 0.95, respectively. Therefore, we can conclude that excellent model correlation with the test data was achieved after model tuning, which lead to a more reliable flutter speed prediction.

Table 6. Summary of center of gravity, moment of inertia, orthonormalized mass matrix and MAC values for the ATW2 before and after model tuning.

		Before tuning			After tuning			
C.G. (X,Y,Z)		14.22, -11.86, -0.011			13.089, -7.61, -0.0080			
Ixx		73.44			97.52			
Iyy		74.74			118.13			
Izz		148.1			215.5			
Ixy		-43.03			-85.55			
Ixz		0.032			0.0286			
Iyz		-0.02			0.0956			
Orthonormalized mass matrix			1	2	3	1	2	3
		1	1	25.0%	4.6%	1	4.0%	-5.7%
		2	0.2467	1	37.0%	0.0395	1	-7.4%
		3	0.0463	0.3681	1	-0.0565	-0.0743	1
MAC	Mode 1	0.90			0.99			
	Mode 2	0.52			0.97			
	Mode 3	0.73			0.95			

CONCLUDING REMARKS

This paper describes the ground vibration test (GVT) and model tuning procedures for the second aerostructures test wing (ATW2), which was developed at the National Aeronautics and Space Administration Dryden Flight Research Center (Edwards, California) for demonstrating flutter and advanced aeroelastic test techniques. In the sensor locations selection process, it was found that the effective independence (EI) and the genetic algorithm (GA) gave a higher determinant value of the Fisher information matrix (**FIM**) and thus, should be used for determining the sensor locations.

The finite element (FE) model tuning process was a challenging task, which depended not only on the accuracy of the experimental data, but also required a good prediction of the design variables for the optimization. After tuning the FE model, the frequency differences between GVT and the numerical results were within 3%, and the off-diagonal terms of the orthonormalized mass matrix were within 10%, both of which satisfy the military specifications. Excellent mode shape correlations were also achieved through the high modal assurance criterion (MAC) value (greater than 95%). With the updated FE model, the accuracy of flutter analysis can be improved and the flutter boundary prediction will be more reliable.

REFERENCES

1. Lind, Rick, David Voracek, Roger Truax, Tim Doyle, Starr Potter, and Marty Brenner, "A Flight Test to Demonstrate Flutter and Evaluate the Flutterometer," *The Aeronautical Journal*, Vol. 107, No. 1076, pp. 577 – 588, October 2003.
2. Pak, Chan-gi, and Wesley Li, "Multidisciplinary Design, Analysis, and Optimization Tool Development Using a Genetic Algorithm," *Proceedings of the 26th Congress of International Council of the Aeronautical Science*, Anchorage, 2008.
3. Kammer, Daniel C., "Sensor Placement for On-Orbit Modal Identification and Correlation of Large Space Structures," *AIAA Journal of Guidance, Control and Dynamics*, Vol. 14, No. 2, pp. 251-259, 1991.
4. Charbonneau, Paul, and Barry Knapp, *A User's Guide to PIKAIA 1.0*, National Center for Atmospheric Research, Boulder, CO, 1995.
5. Friswell, M. I., and J. E. Mottershead, *Finite Element Model Updating in Structural Dynamics*, Kluwer Academic Publishers, Dordrecht, 1995.
6. Guyan, Robert J., "Reduction of Stiffness and Mass Matrices," *AIAA Journal*, Vol. 3, No. 2, p. 380, 1965.
7. Tinker, Michael L., "Accelerometer Placement for the International Space Station Node Modal Test," AIAA-1998-2078, *AIAA/ASME/ASCE/AHS/ASC Structures, Structural Dynamics, and Materials Conference and Exhibit, 39th and AIAA/ASME/AHS Adaptive Structures Forum*, Long Beach, CA, April 20-23, 1998.
8. EI-Borgi, S., M. Neifar, F. Cherif, S. Choura, and H. Smaoui, "Modal Identification, Model Updating and Nonlinear Analysis of a Reinforced Concrete Bridge," *Journal of Vibration and Control*, Vol. 14, No. 4, pp. 511-530, 2008.
9. Pak, Chan-gi, "Finite Element Model Tuning Using Measured Mass Properties and Ground Vibration Test Data," *ASME Journal of Vibration and Acoustics*, Vol. 131, No. 1, February 2009.
10. Lung, Shun-fat, and Chan-gi Pak, "Structural Model Tuning Capability in an Object-Oriented Multidisciplinary Design, Analysis, and Optimization Tool," *Proceedings of the 26th Congress of International Council of the Aeronautical Sciences*, Anchorage, 2008.
11. Herrera, Claudia Y., and Chan-gi Pak, "Build-up Approach to Updating the Mock Quiet Spike Beam Model," AIAA-2007-1776, *Proceedings of the 48th AIAA/ASME/ASCE/AHS/ASC Structures, Structural Dynamics, and Materials Conference*, Honolulu, Hawaii, April 23-26, 2007.
12. Vanderplaats, Garret N., *Numerical Optimization Techniques for Engineering Design*, 3rd ed., Vanderplaats Research & Development, Inc. 2001.
13. Yeniay, Özgür, "Penalty Function Methods For Constrained Optimization Using Genetic Algorithms," *Mathematical and Computational Applications*, Vol. 10, No. 1, pp. 45-56, 2005.
14. O'Callahan, John C., "A New Procedure for an Improved Reduced System (IRS) Model," *Proceedings of the 7th International Modal Analysis Conference*, Vol. 1, pp. 17-21, Las Vegas, 1989.

15. O'Callahan, J. C., P. Avitabile, and R. Riemer, "System Equivalent Reduction Expansion Process," *Proceedings of the 7th International Modal Analysis Conference*, Vol. 1, pp. 29-37, Las Vegas, 1989.
16. *PONTOS User Manual Version 6.0*, Gesellschaft für Optische Messtechnik, Braunschweig, Germany, 2007.
17. Juang, Jer-Nan, and Richard S. Pappa, "An Eigensystem Realization Algorithm for Modal Parameter Identification and Modal Reduction," *AIAA Journal of Guidance, Control, and Dynamics*, Vol. 8, No. 5, pp. 620-627, 1984.
18. MSC.Software Corporation, *MSC.Nastran 2005 Quick Reference Guide: Volume 1*, MSC.Software Corporation, 2005.
19. *Test Requirements for Launch, Upper-Stage, and Space Vehicles*, MIL-STD-1540C Section 6.2.10, September 15, 1994.
20. Norton, William J., *Structures Flight Test Handbook*, AFFTC-TIH-90-001, November 1990.

APPENDIX

THE FE MODEL IN THE MSC/NASTRAN FORMAT

```

$ NASTRAN input file created by the MSC MSC.Nastran input file
$ translator ( MSC.Patran 13.1.116 ) on December 13, 2007 at 08:05:41.
ASSIGN OUTPUT4='atw2c_maa.op4',UNIT=30,STATUS=UNKNOWN,FORM=FORMATTED
ASSIGN OUTPUT4='atw2c_kaa.op4',UNIT=31,STATUS=UNKNOWN,FORM=FORMATTED
SOL 103
$ Direct Text Input for Executive Control
$=====
$ DMAP ALTER SOL 103
    COMPILE SEMODES SOUIN=MSCSOU LIST REF$
    ALTER 315$
    OUTPUT4 MAA///30/2//9$
    OUTPUT4 KAA///31/2//9$
    ENDALTER
$=====
CEND
SEALL = ALL
SUPER = ALL
TITLE = ATW2
$ECHO = SORT
$ Direct Text Input for Global Case Control Data
SUBCASE 1
$ Subcase name : ATW2C
    SUBTITLE=ATW2C
    METHOD = 1
    SPC = 2
$ VECTOR(PLOT, SORT1, REAL)=ALL
    DISP=ALL
GPKE = ALL
BEGIN BULK
PARAM POST -1
PARAM AUTOSPC YES
PARAM WTMASS .002588
PARAM GRDPNT 0
PARAM NOCOMPS,-1
PARAM, USETPRT, 10
EIGRL 1 10 0 MAX
$ Direct Text Input for Bulk Data
$ Elements and Element Properties for region : pbar.700
PBAR 700 701 .5 .1 .1
$ Pset: "pbar.700" will be imported as: "pbar.700"
CBAR 300 700 303 308 -.061556-.998102.0018318
CBAR 301 700 9 124 -.061556-.998102.0018318
$ Elements and Element Properties for region : pcomp.500
$ Composite Property Record created from P3/PATRAN composite material
$ record : pcomp.500
$ Composite Material Description :
PCOMP 500 .01 0. 0.
      501 .01 45. YES 501 .01 -45. YES
$ Pset: "pcomp.500" will be imported as: "pcomp.500"
CQUAD4 500 500 229 240 113 102 0. 0.
CQUAD4 501 500 218 229 102 91 0. 0.

```

CQUAD4	502	500	207	218	91	80	0.	0.
CQUAD4	503	500	196	207	80	69	0.	0.
CQUAD4	504	500	185	196	69	58	0.	0.
CQUAD4	505	500	174	185	58	47	0.	0.
CQUAD4	506	500	163	174	47	36	0.	0.
CQUAD4	507	500	152	163	36	25	0.	0.
CQUAD4	508	500	141	152	25	14	0.	0.
CQUAD4	509	500	130	141	14	3	0.	0.
CQUAD4	510	500	227	104	115	238	0.	0.
CQUAD4	511	500	216	93	104	227	0.	0.
CQUAD4	512	500	205	82	93	216	0.	0.
CQUAD4	513	500	194	71	82	205	0.	0.
CQUAD4	514	500	183	60	71	194	0.	0.
CQUAD4	515	500	172	49	60	183	0.	0.
CQUAD4	516	500	161	38	49	172	0.	0.
CQUAD4	517	500	150	27	38	161	0.	0.
CQUAD4	518	500	139	16	27	150	0.	0.
CQUAD4	519	500	128	5	16	139	0.	0.

\$ Elements and Element Properties for region : celas2.ca6.cb6
PELAS 1 50.
\$ Pset: "celas2.ca6.cb6" will be imported as: "pelas.1"
CELAS1 302 1 9 6 303 6
\$ Elements and Element Properties for region : pelas.2
PELAS 2 1.+8
\$ Pset: "pelas.2" will be imported as: "pelas.2"
CELAS1 4006 2 403 6 402 6
\$ Elements and Element Properties for region : celas2.ca5.cb5
PELAS 3 1.+8
\$ Pset: "celas2.ca5.cb5" will be imported as: "pelas.3"
CELAS1 4005 3 403 5 402 5
\$ Elements and Element Properties for region : celas2.ca4.cb4
PELAS 4 1.+8
\$ Pset: "celas2.ca4.cb4" will be imported as: "pelas.4"
CELAS1 4004 4 403 4 402 4
\$ Elements and Element Properties for region : celas2.ca3.cb3
PELAS 5 1.+6
\$ Pset: "celas2.ca3.cb3" will be imported as: "pelas.5"
CELAS1 4003 5 403 3 402 3
\$ Elements and Element Properties for region : celas2.ca2.cb2
PELAS 6 1.+6
\$ Pset: "celas2.ca2.cb2" will be imported as: "pelas.6"
CELAS1 4002 6 403 2 402 2
\$ Elements and Element Properties for region : celas2.ca1.cb1
PELAS 7 1.+6
\$ Pset: "celas2.ca1.cb1" will be imported as: "pelas.7"
CELAS1 4001 7 403 1 402 1
\$ Elements and Element Properties for region : pshell.600
PSHELL 600 601 .03 601 601
\$ Pset: "pshell.600" will be imported as: "pshell.600"
CTRIA3 600 600 241 111 112 0. 0.
CQUAD4 601 600 240 241 112 113 0. 0.
CQUAD4 602 600 239 240 113 114 0. 0.
CQUAD4 603 600 238 239 114 115 0. 0.
CQUAD4 604 600 237 238 115 116 0. 0.
CQUAD4 605 600 236 237 116 117 0. 0.
CQUAD4 606 600 235 236 117 118 0. 0.
CQUAD4 607 600 234 235 118 119 0. 0.

CQUAD4	608	600	233	234	119	120	0.	0.
CTRIA3	609	600	121	233	120	0.	0.	
CTRIA3	610	600	219	89	90	0.	0.	
CQUAD4	611	600	218	219	90	91	0.	0.
CQUAD4	612	600	217	218	91	92	0.	0.
CQUAD4	613	600	216	217	92	93	0.	0.
CQUAD4	614	600	215	216	93	94	0.	0.
CQUAD4	615	600	214	215	94	95	0.	0.
CQUAD4	616	600	213	214	95	96	0.	0.
CQUAD4	617	600	212	213	96	97	0.	0.
CQUAD4	618	600	211	212	97	98	0.	0.
CTRIA3	619	600	99	211	98	0.	0.	
CTRIA3	620	600	197	67	68	0.	0.	
CQUAD4	621	600	196	197	68	69	0.	0.
CQUAD4	622	600	195	196	69	70	0.	0.
CQUAD4	623	600	194	195	70	71	0.	0.
CQUAD4	624	600	193	194	71	72	0.	0.
CQUAD4	625	600	192	193	72	73	0.	0.
CQUAD4	626	600	191	192	73	74	0.	0.
CQUAD4	627	600	190	191	74	75	0.	0.
CQUAD4	628	600	189	190	75	76	0.	0.
CTRIA3	629	600	77	189	76	0.	0.	
CTRIA3	630	600	175	45	46	0.	0.	
CQUAD4	631	600	174	175	46	47	0.	0.
CQUAD4	632	600	173	174	47	48	0.	0.
CQUAD4	633	600	172	173	48	49	0.	0.
CQUAD4	634	600	171	172	49	50	0.	0.
CQUAD4	635	600	170	171	50	51	0.	0.
CQUAD4	636	600	169	170	51	52	0.	0.
CQUAD4	637	600	168	169	52	53	0.	0.
CQUAD4	638	600	310	311	305	306	0.	0.
CTRIA3	639	600	307	310	306	0.	0.	
CTRIA3	640	600	153	23	24	0.	0.	
CQUAD4	641	600	152	153	24	25	0.	0.
CQUAD4	642	600	151	152	25	26	0.	0.
CQUAD4	643	600	150	151	26	27	0.	0.
CQUAD4	644	600	149	150	27	28	0.	0.
CQUAD4	645	600	148	149	28	29	0.	0.
CQUAD4	646	600	147	148	29	30	0.	0.
CQUAD4	647	600	146	147	30	31	0.	0.
CQUAD4	648	600	314	308	303	313	0.	0.
CTRIA3	649	600	312	314	313	0.	0.	
CTRIA3	650	600	131	1	2	0.	0.	
CQUAD4	651	600	130	131	2	3	0.	0.
CQUAD4	652	600	129	130	3	4	0.	0.
CQUAD4	653	600	128	129	4	5	0.	0.
CQUAD4	654	600	127	128	5	6	0.	0.
CQUAD4	655	600	126	127	6	7	0.	0.
CQUAD4	656	600	125	126	7	8	0.	0.
CQUAD4	657	600	124	125	8	9	0.	0.
CQUAD4	658	600	123	124	9	10	0.	0.
CTRIA3	659	600	11	123	10	0.	0.	
CQUAD4	660	600	145	146	31	32	0.	0.
CTRIA3	661	600	33	145	32	0.	0.	
CQUAD4	662	600	167	168	53	54	0.	0.
CTRIA3	663	600	55	167	54	0.	0.	

\$ Elements and Element Properties for region : pshell.608

```

PSHELL  608    601    .06    601          601
$ Pset: "pshell.608" will be imported as: "pshell.608"
CQUAD4  700    608    309    311    305    304    0.    0.
CQUAD4  701    608    308    309    304    303    0.    0.
CQUAD4  702    608    31     42    157    146    0.    0.
CQUAD4  703    608    42     53    168    157    0.    0.
$ Elements and Element Properties for region : psolid.300
PSOLID  300    301    0
$ Pset: "psolid.300" will be imported as: "psolid.300"
CHEXA   200    300    13     2     3     14    142   131
        130    141
CHEXA   201    300    14     3     4     15    141   130
        129    140
CHEXA   202    300    24     13    14     25    153   142
        141    152
CHEXA   203    300    15     4     5     16    140   129
        128    139
CHEXA   204    300    25     14    15     26    152   141
        140    151
CHEXA   205    300    35     24    25     36    164   153
        152    163
CHEXA   206    300    16     5     6     17    139   128
        127    138
CHEXA   207    300    26     15    16     27    151   140
        139    150
CHEXA   208    300    36     25    26     37    163   152
        151    162
CHEXA   209    300    46     35    36     47    175   164
        163    174
CHEXA   210    300    17     6     7     18    138   127
        126    137
CHEXA   211    300    27     16    17     28    150   139
        138    149
CHEXA   212    300    37     26    27     38    162   151
        150    161
CHEXA   213    300    47     36    37     48    174   163
        162    173
CHEXA   214    300    57     46    47     58    186   175
        174    185
CHEXA   215    300    18     7     8     19    137   126
        125    136
CHEXA   216    300    28     17    18     29    149   138
        137    148
CHEXA   217    300    38     27    28     39    161   150
        149    160
CHEXA   218    300    48     37    38     49    173   162
        161    172
CHEXA   219    300    58     47    48     59    185   174
        173    184
CHEXA   220    300    68     57    58     69    197   186
        185    196
CHEXA   221    300    19     8     9     20    136   125
        124    135
CHEXA   222    300    29     18    19     30    148   137
        136    147
CHEXA   223    300    39     28    29     40    160   149
        148    159

```


CHEXA	224	300	49	38	39	50	172	161
	160	171						
CHEXA	225	300	59	48	49	60	184	173
	172	183						
CHEXA	226	300	69	58	59	70	196	185
	184	195						
CHEXA	227	300	79	68	69	80	208	197
	196	207						
CHEXA	228	300	20	9	10	21	135	124
	123	134						
CHEXA	229	300	30	19	20	31	147	136
	135	146						
CHEXA	230	300	40	29	30	41	159	148
	147	158						
CHEXA	231	300	50	39	40	51	171	160
	159	170						
CHEXA	232	300	60	49	50	61	183	172
	171	182						
CHEXA	233	300	70	59	60	71	195	184
	183	194						
CHEXA	234	300	80	69	70	81	207	196
	195	206						
CHEXA	235	300	90	79	80	91	219	208
	207	218						
CHEXA	236	300	31	20	21	32	146	135
	134	145						
CHEXA	237	300	41	30	31	42	158	147
	146	157						
CHEXA	238	300	51	40	41	52	170	159
	158	169						
CHEXA	239	300	61	50	51	62	182	171
	170	181						
CHEXA	240	300	71	60	61	72	194	183
	182	193						
CHEXA	241	300	81	70	71	82	206	195
	194	205						
CHEXA	242	300	91	80	81	92	218	207
	206	217						
CHEXA	243	300	101	90	91	102	230	219
	218	229						
CHEXA	244	300	304	303	313	300	309	308
	314	302						
CHEXA	245	300	52	41	42	53	169	158
	157	168						
CHEXA	246	300	62	51	52	63	181	170
	169	180						
CHEXA	247	300	72	61	62	73	193	182
	181	192						
CHEXA	248	300	82	71	72	83	205	194
	193	204						
CHEXA	249	300	92	81	82	93	217	206
	205	216						
CHEXA	250	300	102	91	92	103	229	218
	217	228						
CHEXA	251	300	112	101	102	113	241	230
	229	240						
CHEXA	252	300	305	304	300	306	311	309

	302	310							
CHEXA	253	300	63	52	53	64	180	169	
	168	179							
CHEXA	254	300	73	62	63	74	192	181	
	180	191							
CHEXA	255	300	83	72	73	84	204	193	
	192	203							
CHEXA	256	300	93	82	83	94	216	205	
	204	215							
CHEXA	257	300	103	92	93	104	228	217	
	216	227							
CHEXA	258	300	113	102	103	114	240	229	
	228	239							
CHEXA	259	300	64	53	54	65	179	168	
	167	178							
CHEXA	260	300	74	63	64	75	191	180	
	179	190							
CHEXA	261	300	84	73	74	85	203	192	
	191	202							
CHEXA	262	300	94	83	84	95	215	204	
	203	214							
CHEXA	263	300	104	93	94	105	227	216	
	215	226							
CHEXA	264	300	114	103	104	115	239	228	
	227	238							
CHEXA	265	300	75	64	65	76	190	179	
	178	189							
CHEXA	266	300	85	74	75	86	202	191	
	190	201							
CHEXA	267	300	95	84	85	96	214	203	
	202	213							
CHEXA	268	300	105	94	95	106	226	215	
	214	225							
CHEXA	269	300	115	104	105	116	238	227	
	226	237							
CHEXA	270	300	86	75	76	87	201	190	
	189	200							
CHEXA	271	300	96	85	86	97	213	202	
	201	212							
CHEXA	272	300	106	95	96	107	225	214	
	213	224							
CHEXA	273	300	116	105	106	117	237	226	
	225	236							
CHEXA	274	300	97	86	87	98	212	201	
	200	211							
CHEXA	275	300	107	96	97	108	224	213	
	212	223							
CHEXA	276	300	117	106	107	118	236	225	
	224	235							
CHEXA	277	300	108	97	98	109	223	212	
	211	222							
CHEXA	278	300	118	107	108	119	235	224	
	223	234							
CHEXA	279	300	119	108	109	120	234	223	
	222	233							
CPENTA	280	300	2	1	131	13	12	142	
CPENTA	281	300	13	12	142	24	23	153	

CPENTA	282	300	24	23	153	35	34	164
CPENTA	283	300	35	34	164	46	45	175
CPENTA	284	300	46	45	175	57	56	186
CPENTA	285	300	57	56	186	68	67	197
CPENTA	286	300	68	67	197	79	78	208
CPENTA	287	300	79	78	208	90	89	219
CPENTA	288	300	90	89	219	101	100	230
CPENTA	289	300	21	22	134	10	11	123
CPENTA	290	300	101	100	230	112	111	241
CPENTA	291	300	32	33	145	21	22	134
CPENTA	292	300	300	301	302	313	312	314
CPENTA	293	300	306	307	310	300	301	302
CPENTA	294	300	65	66	178	54	55	167
CPENTA	295	300	76	77	189	65	66	178
CPENTA	296	300	87	88	200	76	77	189
CPENTA	297	300	98	99	211	87	88	200
CPENTA	298	300	109	110	222	98	99	211
CPENTA	299	300	120	121	233	109	110	222

\$ Elements and Element Properties for region : conm2

CONM2	400	500	0	0.475	0.	0.	0.
	0.	0.	0.	0.	0.	0.	
CONM2	401	513	0	0.	0.	0.	0.
	0.	0.	0.	0.	0.	0.	
CONM2	402	529	0	0.075	0.	0.	0.
	0.	0.	0.	0.	0.	0.	
CONM2	406	68	0	0.03	0.	0.	0.
	0.	0.	0.	0.	0.	0.	
CONM2	407	57	0	0.03	0.	0.	0.
	0.	0.	0.	0.	0.	0.	
CONM2	408	46	0	0.03	0.	0.	0.
	0.	0.	0.	0.	0.	0.	
CONM2	409	35	0	0.03	0.	0.	0.
	0.	0.	0.	0.	0.	0.	
CONM2	410	24	0	0.03	0.	0.	0.
	0.	0.	0.	0.	0.	0.	
CONM2	412	91	0	0.0638	0.	0.	0.
	0.	0.	0.	0.	0.	0.	
CONM2	413	97	0	0.0638	0.	0.	0.
	0.	0.	0.	0.	0.	0.	
CONM2	414	103	0	0.0638	0.	0.	0.
	0.	0.	0.	0.	0.	0.	
CONM2	415	109	0	0.0638	0.	0.	0.
	0.	0.	0.	0.	0.	0.	
CONM2	416	212	0	0.0638	0.	0.	0.
	0.	0.	0.	0.	0.	0.	
CONM2	417	218	0	0.0638	0.	0.	0.
	0.	0.	0.	0.	0.	0.	
CONM2	418	228	0	0.0638	0.	0.	0.
	0.	0.	0.	0.	0.	0.	
CONM2	419	222	0	0.0638	0.	0.	0.
	0.	0.	0.	0.	0.	0.	

\$ Elements and Element Properties for region : pbar.39

PBAR	39	901	.097314	.011411	.011411	.022821
	.5		.5	-.5		

-.5

\$ Pset: "pbar.39" will be imported as: "pbar.39"

CBAR	800	39	501	500	0.	-1.	0.
CBAR	801	39	502	501	0.	-1.	0.

CBAR	802	39	503	502	0.	-1.	0.
CBAR	803	39	504	503	0.	-1.	0.
CBAR	804	39	505	504	0.	-1.	0.
CBAR	805	39	506	505	0.	-1.	0.
CBAR	806	39	507	506	0.	-1.	0.
CBAR	807	39	508	507	0.	-1.	0.
CBAR	808	39	509	508	0.	-1.	0.
CBAR	809	39	510	509	0.	-1.	0.
CBAR	810	39	512	511	0.	1.	0.
CBAR	811	39	513	512	0.	1.	0.
CBAR	812	39	514	513	0.	1.	0.
CBAR	813	39	515	514	0.	-1.	0.
CBAR	814	39	516	515	0.	-1.	0.
CBAR	815	39	517	516	0.	-1.	0.
CBAR	816	39	518	517	0.	1.	0.
CBAR	817	39	519	518	0.	-1.	0.
CBAR	818	39	520	519	0.	-1.	0.
CBAR	819	39	521	520	0.	-1.	0.
CBAR	820	39	522	521	0.	-1.	0.
CBAR	821	39	523	522	0.	-1.	0.
CBAR	822	39	524	523	0.	-1.	0.
CBAR	823	39	525	524	0.	-1.	0.
CBAR	824	39	526	525	0.	-1.	0.
CBAR	825	39	527	526	0.	-1.	0.
CBAR	826	39	528	527	0.	-1.	0.
CBAR	827	39	529	528	0.	-1.	0.
CBAR	828	39	530	510	0.	-1.	0.
CBAR	829	39	511	530	0.	1.	0.

\$ Elements and Element Properties for region : pcomp.41

\$ Composite Property Record created from P3/PATRAN composite material

\$ record : pcomp.10

\$ Composite Material Description :

PCOMP	41	-.13		8000.	HOFF	0.	0.	
	201	.11	0.	YES	202	.02	45.	YES

\$ Pset: "pcomp.41" will be imported as: "pcomp.41"

CQUAD4	1002	41	228	239	240	229	4	0.
CQUAD4	1003	41	227	238	239	228	4	0.
CQUAD4	1012	41	217	228	229	218	4	0.
CQUAD4	1013	41	216	227	228	217	4	0.
CQUAD4	1202	41	102	113	114	103	4	0.
CQUAD4	1203	41	103	114	115	104	4	0.
CQUAD4	1212	41	91	102	103	92	4	0.
CQUAD4	1213	41	92	103	104	93	4	0.

\$ Elements and Element Properties for region : pcomp.42

\$ Composite Property Record created from P3/PATRAN composite material

\$ record : pcomp.20

\$ Composite Material Description :

PCOMP	42	-.09		8000.	HOFF	0.	0.	
	201	.075	0.	YES	202	.015	45.	YES

\$ Pset: "pcomp.42" will be imported as: "pcomp.42"

CQUAD4	1022	42	206	217	218	207	4	0.
CQUAD4	1023	42	205	216	217	206	4	0.
CQUAD4	1032	42	195	206	207	196	4	0.
CQUAD4	1033	42	194	205	206	195	4	0.
CQUAD4	1222	42	80	91	92	81	4	0.
CQUAD4	1223	42	81	92	93	82	4	0.
CQUAD4	1232	42	69	80	81	70	4	0.

```

CQUAD4 1233 42 70 81 82 71 4 0.
$ Elements and Element Properties for region : pcomp.43
$ Composite Property Record created from P3/PATRAN composite material
$ record : pcomp.30
$ Composite Material Description :
PCOMP 43 -.073 8000. HOFF 0. 0.
      201 .058 0. YES 202 .015 45. YES
$ Pset: "pcomp.43" will be imported as: "pcomp.43"
CQUAD4 1042 43 184 195 196 185 4 0.
CQUAD4 1043 43 183 194 195 184 4 0.
CQUAD4 1052 43 173 184 185 174 4 0.
CQUAD4 1053 43 172 183 184 173 4 0.
CQUAD4 1242 43 58 69 70 59 4 0.
CQUAD4 1243 43 59 70 71 60 4 0.
CQUAD4 1252 43 47 58 59 48 4 0.
CQUAD4 1253 43 48 59 60 49 4 0.
$ Elements and Element Properties for region : pcomp.44
$ Composite Property Record created from P3/PATRAN composite material
$ record : pcomp.40
$ Composite Material Description :
PCOMP 44 -.038 8000. HOFF 0. 0.
      201 .023 0. YES 202 .015 45. YES
$ Pset: "pcomp.44" will be imported as: "pcomp.44"
CQUAD4 1062 44 162 173 174 163 4 0.
CQUAD4 1063 44 161 172 173 162 4 0.
CQUAD4 1072 44 151 162 163 152 4 0.
CQUAD4 1073 44 150 161 162 151 4 0.
CQUAD4 1262 44 36 47 48 37 4 0.
CQUAD4 1263 44 37 48 49 38 4 0.
CQUAD4 1272 44 25 36 37 26 4 0.
CQUAD4 1273 44 26 37 38 27 4 0.
$ Elements and Element Properties for region : pcomp.45
$ Composite Property Record created from P3/PATRAN composite material
$ record : pcomp.50
$ Composite Material Description :
PCOMP 45 -.03 8000. HOFF 0. 0.
      201 .015 0. YES 202 .015 45. YES
$ Pset: "pcomp.45" will be imported as: "pcomp.45"
CQUAD4 1082 45 140 151 152 141 4 0.
CQUAD4 1083 45 139 150 151 140 4 0.
CQUAD4 1092 45 129 140 141 130 4 0.
CQUAD4 1093 45 128 139 140 129 4 0.
CQUAD4 1282 45 14 25 26 15 4 0.
CQUAD4 1283 45 15 26 27 16 4 0.
CQUAD4 1292 45 3 14 15 4 4 0.
CQUAD4 1293 45 4 15 16 5 4 0.
$ Elements and Element Properties for region : pcomp.46
$ Composite Property Record created from P3/PATRAN composite material
$ record : pcomp.200
$ Composite Material Description :
PCOMP 46 -.0165 8000. HOFF 0. 0.
      202 .0033 45. YES 202 .0033 -45. YES
      202 .0033 45. YES 202 .0033 -45. YES
      202 .0033 45. YES
$ Pset: "pcomp.46" will be imported as: "pcomp.46"
CQUAD4 1000 46 230 241 111 100 4 0.
CQUAD4 1001 46 229 240 241 230 4 0.

```

CQUAD4	1004	46	226	237	238	227	4	0.
CQUAD4	1005	46	225	236	237	226	4	0.
CQUAD4	1006	46	224	235	236	225	4	0.
CQUAD4	1007	46	223	234	235	224	4	0.
CQUAD4	1008	46	222	233	234	223	4	0.
CQUAD4	1009	46	110	121	233	222	4	0.
CQUAD4	1010	46	219	230	100	89	4	0.
CQUAD4	1011	46	218	229	230	219	4	0.
CQUAD4	1014	46	215	226	227	216	4	0.
CQUAD4	1015	46	214	225	226	215	4	0.
CQUAD4	1016	46	213	224	225	214	4	0.
CQUAD4	1017	46	212	223	224	213	4	0.
CQUAD4	1018	46	211	222	223	212	4	0.
CQUAD4	1019	46	99	110	222	211	4	0.
CQUAD4	1020	46	208	219	89	78	4	0.
CQUAD4	1021	46	207	218	219	208	4	0.
CQUAD4	1024	46	204	215	216	205	4	0.
CQUAD4	1025	46	203	214	215	204	4	0.
CQUAD4	1026	46	202	213	214	203	4	0.
CQUAD4	1027	46	201	212	213	202	4	0.
CQUAD4	1028	46	200	211	212	201	4	0.
CQUAD4	1029	46	88	99	211	200	4	0.
CQUAD4	1030	46	197	208	78	67	4	0.
CQUAD4	1031	46	196	207	208	197	4	0.
CQUAD4	1034	46	193	204	205	194	4	0.
CQUAD4	1035	46	192	203	204	193	4	0.
CQUAD4	1036	46	191	202	203	192	4	0.
CQUAD4	1037	46	190	201	202	191	4	0.
CQUAD4	1038	46	189	200	201	190	4	0.
CQUAD4	1039	46	77	88	200	189	4	0.
CQUAD4	1040	46	186	197	67	56	4	0.
CQUAD4	1041	46	185	196	197	186	4	0.
CQUAD4	1044	46	182	193	194	183	4	0.
CQUAD4	1045	46	181	192	193	182	4	0.
CQUAD4	1046	46	180	191	192	181	4	0.
CQUAD4	1047	46	179	190	191	180	4	0.
CQUAD4	1048	46	178	189	190	179	4	0.
CQUAD4	1049	46	66	77	189	178	4	0.
CQUAD4	1050	46	175	186	56	45	4	0.
CQUAD4	1051	46	174	185	186	175	4	0.
CQUAD4	1054	46	171	182	183	172	4	0.
CQUAD4	1055	46	170	181	182	171	4	0.
CQUAD4	1056	46	169	180	181	170	4	0.
CQUAD4	1057	46	168	179	180	169	4	0.
CQUAD4	1058	46	167	178	179	168	4	0.
CQUAD4	1059	46	55	66	178	167	4	0.
CQUAD4	1060	46	164	175	45	34	4	0.
CQUAD4	1061	46	163	174	175	164	4	0.
CQUAD4	1064	46	160	171	172	161	4	0.
CQUAD4	1065	46	159	170	171	160	4	0.
CQUAD4	1066	46	158	169	170	159	4	0.
CQUAD4	1067	46	157	168	169	158	4	0.
CQUAD4	1070	46	153	164	34	23	4	0.
CQUAD4	1071	46	152	163	164	153	4	0.
CQUAD4	1074	46	149	160	161	150	4	0.
CQUAD4	1075	46	148	159	160	149	4	0.
CQUAD4	1076	46	147	158	159	148	4	0.

CQUAD4	1077	46	146	157	158	147	4	0.
CQUAD4	1080	46	142	153	23	12	4	0.
CQUAD4	1081	46	141	152	153	142	4	0.
CQUAD4	1084	46	138	149	150	139	4	0.
CQUAD4	1085	46	137	148	149	138	4	0.
CQUAD4	1086	46	136	147	148	137	4	0.
CQUAD4	1087	46	135	146	147	136	4	0.
CQUAD4	1088	46	134	145	146	135	4	0.
CQUAD4	1089	46	22	33	145	134	4	0.
CQUAD4	1090	46	131	142	12	1	4	0.
CQUAD4	1091	46	130	141	142	131	4	0.
CQUAD4	1094	46	127	138	139	128	4	0.
CQUAD4	1095	46	126	137	138	127	4	0.
CQUAD4	1096	46	125	136	137	126	4	0.
CQUAD4	1097	46	124	135	136	125	4	0.
CQUAD4	1098	46	123	134	135	124	4	0.
CQUAD4	1099	46	11	22	134	123	4	0.
CQUAD4	1200	46	100	111	112	101	4	0.
CQUAD4	1201	46	101	112	113	102	4	0.
CQUAD4	1204	46	104	115	116	105	4	0.
CQUAD4	1205	46	105	116	117	106	4	0.
CQUAD4	1206	46	106	117	118	107	4	0.
CQUAD4	1207	46	107	118	119	108	4	0.
CQUAD4	1208	46	108	119	120	109	4	0.
CQUAD4	1209	46	109	120	121	110	4	0.
CQUAD4	1210	46	89	100	101	90	4	0.
CQUAD4	1211	46	90	101	102	91	4	0.
CQUAD4	1214	46	93	104	105	94	4	0.
CQUAD4	1215	46	94	105	106	95	4	0.
CQUAD4	1216	46	95	106	107	96	4	0.
CQUAD4	1217	46	96	107	108	97	4	0.
CQUAD4	1218	46	97	108	109	98	4	0.
CQUAD4	1219	46	98	109	110	99	4	0.
CQUAD4	1220	46	78	89	90	79	4	0.
CQUAD4	1221	46	79	90	91	80	4	0.
CQUAD4	1224	46	82	93	94	83	4	0.
CQUAD4	1225	46	83	94	95	84	4	0.
CQUAD4	1226	46	84	95	96	85	4	0.
CQUAD4	1227	46	85	96	97	86	4	0.
CQUAD4	1228	46	86	97	98	87	4	0.
CQUAD4	1229	46	87	98	99	88	4	0.
CQUAD4	1230	46	67	78	79	68	4	0.
CQUAD4	1231	46	68	79	80	69	4	0.
CQUAD4	1234	46	71	82	83	72	4	0.
CQUAD4	1235	46	72	83	84	73	4	0.
CQUAD4	1236	46	73	84	85	74	4	0.
CQUAD4	1237	46	74	85	86	75	4	0.
CQUAD4	1238	46	75	86	87	76	4	0.
CQUAD4	1239	46	76	87	88	77	4	0.
CQUAD4	1240	46	56	67	68	57	4	0.
CQUAD4	1241	46	57	68	69	58	4	0.
CQUAD4	1244	46	60	71	72	61	4	0.
CQUAD4	1245	46	61	72	73	62	4	0.
CQUAD4	1246	46	62	73	74	63	4	0.
CQUAD4	1247	46	63	74	75	64	4	0.
CQUAD4	1248	46	64	75	76	65	4	0.
CQUAD4	1249	46	65	76	77	66	4	0.

CQUAD4	1250	46	45	56	57	46	4	0.
CQUAD4	1251	46	46	57	58	47	4	0.
CQUAD4	1254	46	49	60	61	50	4	0.
CQUAD4	1255	46	50	61	62	51	4	0.
CQUAD4	1256	46	51	62	63	52	4	0.
CQUAD4	1257	46	52	63	64	53	4	0.
CQUAD4	1258	46	53	64	65	54	4	0.
CQUAD4	1259	46	54	65	66	55	4	0.
CQUAD4	1260	46	34	45	46	35	4	0.
CQUAD4	1261	46	35	46	47	36	4	0.
CQUAD4	1264	46	38	49	50	39	4	0.
CQUAD4	1265	46	39	50	51	40	4	0.
CQUAD4	1266	46	40	51	52	41	4	0.
CQUAD4	1267	46	41	52	53	42	4	0.
CQUAD4	1270	46	23	34	35	24	4	0.
CQUAD4	1271	46	24	35	36	25	4	0.
CQUAD4	1274	46	27	38	39	28	4	0.
CQUAD4	1275	46	28	39	40	29	4	0.
CQUAD4	1276	46	29	40	41	30	4	0.
CQUAD4	1277	46	30	41	42	31	4	0.
CQUAD4	1280	46	12	23	24	13	4	0.
CQUAD4	1281	46	13	24	25	14	4	0.
CQUAD4	1284	46	16	27	28	17	4	0.
CQUAD4	1285	46	17	28	29	18	4	0.
CQUAD4	1286	46	18	29	30	19	4	0.
CQUAD4	1287	46	19	30	31	20	4	0.
CQUAD4	1288	46	20	31	32	21	4	0.
CQUAD4	1289	46	21	32	33	22	4	0.
CQUAD4	1290	46	1	12	13	2	4	0.
CQUAD4	1291	46	2	13	14	3	4	0.
CQUAD4	1294	46	5	16	17	6	4	0.
CQUAD4	1295	46	6	17	18	7	4	0.
CQUAD4	1296	46	7	18	19	8	4	0.
CQUAD4	1297	46	8	19	20	9	4	0.
CQUAD4	1298	46	9	20	21	10	4	0.
CQUAD4	1299	46	10	21	22	11	4	0.

\$ Elements and Element Properties for region : pshell.47

PSHELL	47	601	.02	601	601			
\$ Pset: "pshell.47" will be imported as: "pshell.47"								
CQUAD4	1068	47	302	310	311	309	4	0.
CQUAD4	1069	47	301	307	310	302	4	0.
CQUAD4	1078	47	314	302	309	308	4	0.
CQUAD4	1079	47	312	301	302	314	4	0.
CQUAD4	1268	47	304	305	306	300	4	0.
CQUAD4	1269	47	300	306	307	301	4	0.
CQUAD4	1278	47	303	304	300	313	4	0.
CQUAD4	1279	47	313	300	301	312	4	0.

\$ Referenced Material Records

\$ Material Record : mat1.301

\$ Description of Material :

MAT1	301	13100.	.499	.0027
------	-----	--------	------	-------

\$ Material Record : mat1.601

\$ Description of Material :

MAT1	601	2.67+6	.483333	.068
------	-----	--------	---------	------

\$ Material Record : mat1.701

\$ Description of Material :

MAT1	701	2.+7	.3
------	-----	------	----


```

$ Material Record : mat1.901
$ Description of Material :
MAT1      901      2.+7          .3          .058
$ Material Record : mat8.201
$ Description of Material :
MAT8      201      1.58+7  1.5+6      .28      1.+6          .058
                218000. 247000. 5850.      35700. 10000.

$ Material Record : mat8.202
$ Description of Material :
MAT8      202      2.67+6  2.67+6          500000.          .068
                43000. 45000. 43000. 45000. 10000.

$ Material Record : mat8.501
$ Description of Material :
MAT8      501      2.67+6  2.67+6  .3          500000.          .068
$ Multipoint Constraints of Group : left_wing
RBE2      303      304      123      42
RBE2      304      303      123      31
RBE2      421      403      123456  112      113      114      115      116
                117      118      119      234      235      236      237      238
                239      240      241
RBE2      4429     518      123456  9         10      123      124
RBE2      4430     511      123456  2         131
RBE2      4431     512      123456  3         130
RBE2      4432     513      123456  4         129
RBE2      4433     514      123456  5         128
RBE2      4434     305      123      53
RBE2      5000     307      123456  55
RBE2      5001     312      123456  33
RBE2      5002     167      123456  310
RBE2      5003     54       123456  306
RBE2      5004     145      123456  314
RBE2      5005     32       123456  313
RBE2      5006     146      123456  308
RBE2      5007     168      123456  311
$ Nodes of Group : left_wing
GRID      1          19.125  -18.      1.57-6
GRID      2          19.9853 -18.      -.104989 3
GRID      3          20.8561 -18.      -.142824 3
GRID      4          21.7274 -18.      -.164471 3
GRID      5          22.5989 -18.      -.173716 3
GRID      6          23.4706 -18.      -.170052
GRID      7          24.3419 -18.      -.151726
GRID      8          25.2129 -18.      -.122049
GRID      9          26.084   -18.      -.084171 5
GRID     10          26.9545 -18.      -.042647 3
GRID     11          27.825   -18.      -7.81-4
GRID     12          17.2125 -16.2     1.41-6
GRID     13          18.1175 -16.2     -.110423
GRID     14          19.0331 -16.2     -.150214
GRID     15          19.9494 -16.2     -.172979
GRID     16          20.8661 -16.2     -.182702
GRID     17          21.7829 -16.2     -.178847
GRID     18          22.6993 -16.2     -.159573
GRID     19          23.6154 -16.2     -.128362
GRID     20          24.5315 -16.2     -.088525
GRID     21          25.447   -16.2     -.044854
GRID     22          26.3624 -16.2     -8.22-4

```

GRID	23	15.3	-14.4	1.25-6	
GRID	24	16.2495	-14.4	-.115857	
GRID	25	17.2103	-14.4	-.157603	
GRID	26	18.1717	-14.4	-.181487	
GRID	27	19.1334	-14.4	-.191687	
GRID	28	20.0952	-14.4	-.187643	
GRID	29	21.0566	-14.4	-.167421	
GRID	30	22.0177	-14.4	-.134674	
GRID	31	22.9789	-14.4	-.09288	3
GRID	32	23.9395	-14.4	-.047061	
GRID	33	24.9	-14.4	-8.62-4	
GRID	34	13.3875	-12.5999	1.1-6	
GRID	35	14.3816	-12.5999	-.121291	
GRID	36	15.3874	-12.5999	-.164993	
GRID	37	16.3939	-12.5999	-.189996	
GRID	38	17.4006	-12.5999	-.200673	
GRID	39	18.4074	-12.5999	-.196439	
GRID	40	19.414	-12.5999	-.175268	
GRID	41	20.4203	-12.5999	-.140986	
GRID	42	21.4263	-12.5999	-.097234	3
GRID	45	11.475	-10.8	9.44-7	
GRID	46	12.5137	-10.8	-.126726	
GRID	47	13.5645	-10.8	-.172384	
GRID	48	14.616	-10.8	-.198504	
GRID	49	15.6679	-10.8	-.209659	
GRID	50	16.7199	-10.8	-.205234	
GRID	51	17.7714	-10.8	-.183115	
GRID	52	18.8227	-10.8	-.147297	
GRID	53	19.8738	-10.7999	-.101589	3
GRID	54	20.9244	-10.7999	-.051475	
GRID	55	21.975	-10.7999	-9.44-4	
GRID	56	9.5625	-9.	7.86-7	
GRID	57	10.6458	-9.	-.132161	
GRID	58	11.7416	-9.	-.179774	
GRID	59	12.8382	-9.	-.207013	
GRID	60	13.9351	-9.	-.218645	
GRID	61	15.0322	-9.	-.21403	
GRID	62	16.1287	-9.	-.190961	
GRID	63	17.2251	-9.	-.153609	
GRID	64	18.3211	-9.	-.105944	
GRID	65	19.4169	-9.	-.053681	
GRID	66	20.5125	-9.	-9.84-4	
GRID	67	7.65	-7.2	6.29-7	
GRID	68	8.77792	-7.2	-.137596	
GRID	69	9.91882	-7.2	-.187164	
GRID	70	11.0604	-7.2	-.215522	
GRID	71	12.2024	-7.2	-.227631	
GRID	72	13.3445	-7.2	-.222825	
GRID	73	14.4862	-7.2	-.198808	
GRID	74	15.6276	-7.2	-.159921	
GRID	75	16.7687	-7.2	-.110298	
GRID	76	17.9093	-7.2	-.055889	
GRID	77	19.0499	-7.2	-.001025	
GRID	78	5.7375	-5.4	4.72-7	
GRID	79	6.91001	-5.4	-.143032	
GRID	80	8.09596	-5.4	-.194555	
GRID	81	9.28267	-5.4	-.224031	

GRID	82	10.4697	-5.4	-.236616	
GRID	83	11.6568	-5.4	-.231621	
GRID	84	12.8436	-5.4	-.206655	
GRID	85	14.03	-5.4	-.166233	
GRID	86	15.2161	-5.4	-.114653	
GRID	87	16.4018	-5.4	-.058096	
GRID	88	17.5875	-5.4	-.001066	
GRID	89	3.825	-3.6	3.14-7	
GRID	90	5.04211	-3.6	-.148468	
GRID	91	6.27309	-3.6	-.201946	
GRID	92	7.50487	-3.6	-.23254	
GRID	93	8.73697	-3.6	-.245602	
GRID	94	9.96917	-3.59999	-.240416	
GRID	95	11.201	-3.59999	-.214501	
GRID	96	12.4324	-3.59999	-.172544	
GRID	97	13.6635	-3.59999	-.119008	
GRID	98	14.8943	-3.59999	-.060303	
GRID	99	16.125	-3.59999	-.001107	
GRID	100	1.91249	-1.79999	1.57-7	
GRID	101	3.17421	-1.79999	-.153904	
GRID	102	4.45024	-1.79999	-.209337	
GRID	103	5.72708	-1.79999	-.241049	
GRID	104	7.00424	-1.79999	-.254588	
GRID	105	8.28149	-1.8	-.249212	
GRID	106	9.55843	-1.8	-.222348	
GRID	107	10.8349	-1.8	-.178856	
GRID	108	12.1109	-1.8	-.123363	
GRID	109	13.3867	-1.8	-.06251	
GRID	110	14.6625	-1.8	-.001147	
GRID	111	0.	0.	0.	
GRID	112	1.30632	-1.39-8	-.159341	3
GRID	113	2.62739	-1.89-8	-.216728	3
GRID	114	3.94929	-2.18-8	-.249558	3
GRID	115	5.27152	-2.3-8	-.263574	3
GRID	116	6.59382	-2.25-8	-.258007	3
GRID	117	7.91583	-2.01-8	-.230194	3
GRID	118	9.23737	-1.61-8	-.185167	3
GRID	119	10.5584	-1.11-8	-.127718	3
GRID	120	11.8792	-5.65-9	-.064717	
GRID	121	13.2	-1.03-10	-.001188	
GRID	123	26.9543	-18.	.042659	3
GRID	124	26.0837	-18.	.084186	3
GRID	125	25.2129	-18.	.122052	
GRID	126	24.3419	-18.	.151729	
GRID	127	23.4705	-18.	.170056	
GRID	128	22.5989	-18.	.173719	3
GRID	129	21.7274	-18.	.164474	3
GRID	130	20.8561	-18.	.142827	3
GRID	131	19.9853	-18.	.104987	3
GRID	134	25.4468	-16.1999	.044865	
GRID	135	24.5312	-16.1999	.08854	
GRID	136	23.6154	-16.1999	.128364	
GRID	137	22.6993	-16.1999	.159576	
GRID	138	21.7828	-16.1999	.178852	
GRID	139	20.8661	-16.1999	.182705	
GRID	140	19.9494	-16.1999	.172982	
GRID	141	19.0331	-16.1999	.150216	

GRID	142	18.1173	-16.1999.11042
GRID	145	23.9393	-14.3999.047071
GRID	146	22.9786	-14.3999.092893
GRID	147	22.0177	-14.3999.134676
GRID	148	21.0566	-14.3999.167423
GRID	149	20.0951	-14.3999.187647
GRID	150	19.1334	-14.3999.19169
GRID	151	18.1717	-14.3999.18149
GRID	152	17.2103	-14.3999.157606
GRID	153	16.2493	-14.3999.115854
GRID	157	21.4261	-12.5999.097247
GRID	158	20.4202	-12.5999.140987
GRID	159	19.414	-12.5999.17527
GRID	160	18.4074	-12.5999.196442
GRID	161	17.4006	-12.5999.200676
GRID	162	16.3939	-12.5999.189999
GRID	163	15.3874	-12.5999.164995
GRID	164	14.3815	-12.5999.121288
GRID	167	20.9242	-10.7999.051483
GRID	168	19.8735	-10.7999.1016
GRID	169	18.8227	-10.7999.147299
GRID	170	17.7714	-10.7999.183116
GRID	171	16.7197	-10.7999.205237
GRID	172	15.6679	-10.7999.209661
GRID	173	14.616	-10.7999.198507
GRID	174	13.5645	-10.7999.172385
GRID	175	12.5136	-10.7999.126723
GRID	178	19.4167	-8.99993.053689
GRID	179	18.3209	-8.99993.105953
GRID	180	17.2251	-8.99994.153611
GRID	181	16.1287	-8.99995.190963
GRID	182	15.032	-8.99996.214033
GRID	183	13.9351	-8.99996.218647
GRID	184	12.8382	-8.99997.207015
GRID	185	11.7416	-8.99998.179775
GRID	186	10.6457	-8.99999.132158
GRID	189	17.9092	-7.19992.055895
GRID	190	16.7684	-7.19993.110306
GRID	191	15.6275	-7.19994.159922
GRID	192	14.4861	-7.19995.19881
GRID	193	13.3444	-7.19996.222828
GRID	194	12.2024	-7.19996.227632
GRID	195	11.0604	-7.19997.215523
GRID	196	9.91878	-7.19998.187165
GRID	197	8.77783	-7.19999.137593
GRID	200	16.4016	-5.39992.0581
GRID	201	15.2159	-5.39993.11466
GRID	202	14.0299	-5.39994.166234
GRID	203	12.8435	-5.39995.206656
GRID	204	11.6567	-5.39995.231623
GRID	205	10.4696	-5.39996.236618
GRID	206	9.28263	-5.39997.224032
GRID	207	8.0959	-5.39998.194555
GRID	208	6.90992	-5.39999.143028
GRID	211	14.8941	-3.59992.060306
GRID	212	13.6634	-3.59993.119013
GRID	213	12.4324	-3.59993.172545

GRID	214	11.2009	-3.59994	.214503	
GRID	215	9.96907	-3.59995	.240418	
GRID	216	8.73691	-3.59996	.245603	
GRID	217	7.50482	-3.59997	.23254	
GRID	218	6.27304	-3.59998	.201945	
GRID	219	5.04203	-3.59999	.148464	
GRID	222	13.3866	-1.79991	.062512	
GRID	223	12.1108	-1.79992	.123366	
GRID	224	10.8348	-1.79993	.178857	
GRID	225	9.55836	-1.79994	.222349	
GRID	226	8.2814	-1.79995	.249213	
GRID	227	7.00418	-1.79996	.254589	
GRID	228	5.72702	-1.79997	.241049	
GRID	229	4.45017	-1.79998	.209336	
GRID	230	3.17414	-1.79999	.153901	
GRID	233	11.8792	5.65-9	.064717	
GRID	234	10.5584	1.11-8	.127719	3
GRID	235	9.23735	1.61-8	.185168	3
GRID	236	7.9158	2.01-8	.230195	3
GRID	237	6.59378	2.25-8	.258007	3
GRID	238	5.27148	2.3-8	.263574	3
GRID	239	3.94924	2.18-8	.249557	3
GRID	240	2.62734	1.89-8	.216727	3
GRID	241	1.30626	1.39-8	.159337	3
GRID	300	22.4319	-12.5999-	.049268	
GRID	301	23.4375	-12.5999-	9.03-4	
GRID	302	22.4317	-12.5999.	0.049277	
GRID	303	22.9789	-14.4	-.09288	5
GRID	304	21.4263	-12.5999-	.097234	5
GRID	305	19.8738	-10.7999-	.101589	5
GRID	306	20.9244	-10.7999-	.051475	
GRID	307	21.975	-10.7999-	9.44-4	
GRID	308	22.9786	-14.3999.	0.092893	
GRID	309	21.4261	-12.5999.	0.097247	
GRID	310	20.9242	-10.7999.	0.051483	
GRID	311	19.8735	-10.7999.	0.1016	
GRID	312	24.9	-14.4	-8.62-4	
GRID	313	23.9395	-14.4	-.047061	
GRID	314	23.9393	-14.3999.	0.047071	
GRID	402	3.94929	0.	0.	3
GRID	403	3.94929	0.	0.	3
GRID	500	12.75	-18.5	0.	
GRID	501	14.50	-18.5	1.57-7	
GRID	502	15.125	-18.5	3.14-7	
GRID	503	15.625	-18.5	4.71-7	
GRID	504	16.125	-18.5	6.28-7	
GRID	505	16.50	-18.5	7.85-7	
GRID	506	17.125	-18.5	9.42-7	
GRID	507	17.625	-18.5	1.09-6	
GRID	508	18.125	-18.5	1.25-6	
GRID	509	18.625	-18.5	1.41-6	
GRID	510	19.125	-18.5	1.57-6	
GRID	511	20.0569	-18.5	1.46-6	3
GRID	512	20.9888	-18.5	1.35-6	3
GRID	513	21.9207	-18.5	1.24-6	3
GRID	514	22.8526	-18.5	1.14-6	3
GRID	515	23.7845	-18.5	1.03-6	

```

GRID      516          24.7164 -18.5   9.29-7
GRID      517          25.6483 -18.5   8.22-7
GRID      518          26.7366 -18.5   6.97-7   3
GRID      519          27.825  -18.5   5.72-7
GRID      520          28.325  -18.5   5.15-7
GRID      521          28.825  -18.5   4.58-7
GRID      522          29.325  -18.5   4.01-7
GRID      523          29.825  -18.5   3.43-7
GRID      524          30.325  -18.5   2.86-7
GRID      525          30.825  -18.5   2.29-7
GRID      526          31.325  -18.5   1.71-7
GRID      527          31.825  -18.5   1.14-7
GRID      528          32.325  -18.5   5.72-8
GRID      529          32.825  -18.5    0.
GRID      530          19.5909 -18.5   1.51-6
$ Loads for Load Case :
SPCADD    2          100
$ Displacement Constraints of Load Set : spc1.100
SPC1      100      123456  402
$ Referenced Coordinate Frames
CORD2R    3          0.      0.      0.      0.      0.      1.
          -1.      0.      0.
CORD2R    4          0.      0.      0.      -.707107-.707107-3.079-8
          -.707107.707107 3.079-8
CORD2R    5          19.8738 -10.7999-.10158934.647 -27.9279-.060154
          2.77994 -25.547 -1.49394
$
$ASET1    3          12      22      23      34      45      56
$ASET1    3          66      67      77      78      88      89
$ASET1    3          99      100     110     111     121     500
$ASET1    3          510     529
ENDDATA  b46081d2

```

REPORT DOCUMENTATION PAGE

*Form Approved
OMB No. 0704-0188*

The public reporting burden for this collection of information is estimated to average 1 hour per response, including the time for reviewing instructions, searching existing data sources, gathering and maintaining the data needed, and completing and reviewing the collection of information. Send comments regarding this burden estimate or any other aspect of this collection of information, including suggestions for reducing this burden, to Department of Defense, Washington Headquarters Services, Directorate for Information Operations and Reports (0704-0188), 1215 Jefferson Davis Highway, Suite 1204, Arlington, VA 22202-4302. Respondents should be aware that notwithstanding any other provision of law, no person shall be subject to any penalty for failing to comply with a collection of information if it does not display a currently valid OMB control number.

PLEASE DO NOT RETURN YOUR FORM TO THE ABOVE ADDRESS.

1. REPORT DATE (DD-MM-YYYY) 01-04-2009		2. REPORT TYPE Technical Memorandum		3. DATES COVERED (From - To)	
4. TITLE AND SUBTITLE Updating the Finite Element Model of the Aerostructures Test Wing Using Ground Vibration Test Data				5a. CONTRACT NUMBER	
				5b. GRANT NUMBER	
				5c. PROGRAM ELEMENT NUMBER	
6. AUTHOR(S) Lung, Shun-Fat and Pak, Chan-Gi				5d. PROJECT NUMBER	
				5e. TASK NUMBER	
				5f. WORK UNIT NUMBER	
7. PERFORMING ORGANIZATION NAME(S) AND ADDRESS(ES) NASA Dryden Flight Research Center P.O. Box 273 Edwards, California 93523-0273				8. PERFORMING ORGANIZATION REPORT NUMBER H-2942	
9. SPONSORING/MONITORING AGENCY NAME(S) AND ADDRESS(ES) National Aeronautics and Space Administration Washington, DC 20546-0001				10. SPONSORING/MONITOR'S ACRONYM(S) NASA	
				11. SPONSORING/MONITORING REPORT NUMBER NASA/TM-2009-214646	
12. DISTRIBUTION/AVAILABILITY STATEMENT Unclassified -- Unlimited Subject Category 01 Availability: NASA CASI (301) 621-0390 Distribution: Standard					
13. SUPPLEMENTARY NOTES Lung, TYBRIN, Inc.; Pak, NASA Dryden Flight Research Center. An Electronic version can be found at http://dtrs.dfr.nasa.gov or http://ntrs.nasa.gov/search.jsp					
14. ABSTRACT Improved and/or accelerated decision making is a crucial step during flutter certification processes. Unfortunately, most finite element structural dynamics models have uncertainties associated with model validity. Tuning the finite element model using measured data to minimize the model uncertainties is a challenging task in the area of structural dynamics. The model tuning process requires not only satisfactory correlations between analytical and experimental results, but also the retention of the mass and stiffness properties of the structures. Minimizing the difference between analytical and experimental results is a type of optimization problem. By utilizing the multidisciplinary design, analysis, and optimization (MDAO) tool in order to optimize the objective function and constraints; the mass properties, the natural frequencies, and the mode shapes can be matched to the target data to retain the mass matrix orthogonality. This approach has been applied to minimize the model uncertainties for the structural dynamics model of the aerostructures test wing (ATW), which was designed and tested at the National Aeronautics and Space Administration Dryden Flight Research Center (Edwards, California). This study has shown that natural frequencies and corresponding mode shapes from the updated finite element model have excellent agreement with corresponding measured data.					
15. SUBJECT TERMS Aerostructures test wing, Ground vibration test, Multidisciplinary design, analysis, and optimization, Structural dynamic model tuning, Sensor/Actuator placement					
16. SECURITY CLASSIFICATION OF:			17. LIMITATION OF ABSTRACT	18. NUMBER OF PAGES	19a. NAME OF RESPONSIBLE PERSON
a. REPORT	b. ABSTRACT	c. THIS PAGE			STI Help Desk (email:help@sti.nasa.gov)
U	U	U	UU	43	19b. TELEPHONE NUMBER (Include area code) (301) 621-0390